The Astrophysical Journal Supplement Series, 166:351–377, 2006 September

SPITZER IRS SPECTROSCOPY OF *IRAS*-DISCOVERED DEBRIS DISKS[1]

C. H. Chen,[2,3] B. A. Sargent,[4] C. Bohac,[4] K. H. Kim,[4] E. Leibensperger,[5] M. Jura,[6] J. Najita,[2]
W. J. Forrest,[4] D. M. Watson,[4] G. C. Sloan,[7] and L. D. Keller[5]
Received 2006 March 3; accepted 2006 May 11

ABSTRACT

We have obtained *Spitzer Space Telescope* Infrared Spectrograph (IRS) 5.5–35 μm spectra of 59 main-sequence stars that possess *IRAS* 60 μm excess. The spectra of five objects possess spectral features that are well-modeled using micron-sized grains and silicates with crystalline mass fractions 0%–80%, consistent with T Tauri and Herbig AeBe stars. With the exception of η Crv, these objects are young with ages $\leq$50 Myr. Our fits require the presence of a cool blackbody continuum, $T_{\rm gr} = 80-200$ K, in addition to hot, amorphous, and crystalline silicates, $T_{\rm gr} = 290-600$ K, suggesting that multiple parent body belts are present in some debris disks, analogous to the asteroid and Kuiper belts in our solar system. The spectra for the majority of objects are featureless, suggesting that the emitting grains probably have radii $a > 10$ μm. We have modeled the excess continua using a continuous disk with a uniform surface density distribution, expected if Poynting-Robertson and stellar wind drag are the dominant grain removal processes, and using a single-temperature blackbody, expected if the dust is located in a narrow ring around the star. The IRS spectra of many objects are better modeled with a single-temperature blackbody, suggesting that the disks possess inner holes. The distribution of grain temperatures, based on our blackbody fits, peaks at $T_{\rm gr} = 110-120$ K. Since the timescale for ice sublimation of micron-sized grains with $T_{\rm gr} > 110$ K is a fraction of a Myr, the lack of warmer material may be explained if the grains are icy. If planets dynamically clear the central portions of debris disks, then the frequency of planets around other stars is probably high. We estimate that the majority of debris disk systems possess parent body masses, $M_{\rm PB} < 1$ $M_{\oplus}$. The low inferred parent body masses suggest that planet formation is an efficient process.

Subject headings: circumstellar matter — infrared: stars — planetary systems: formation

1. INTRODUCTION

Giant planets are believed to form in circumstellar disks by either (1) growth of interstellar grains into planetary cores and subsequent accretion of gas into planetary atmospheres (Pollack et al. 1996) or (2) direct collapse via gravitational instabilities. In the core-accretion model, the first step toward building planets is the growth of small bodies from submicron interstellar grains into meter-sized bodies. Fits of the 10 μm silicate features observed toward pre–main-sequence T Tauri and Herbig AeBe stars suggest that the grains in these systems have grown to radii of a few μm at ages <few Myr (Forrest et al. 2004; Uchida et al. 2004; Honda et al. 2003; Bouwman et al. 2001). However, how and when micron-sized grains grow to kilometer-sized planetesimals, and the efficiency of this process, are not well constrained. Mid-infrared spectroscopy of debris disks around main-sequence stars may be used to detect larger grains and to infer the presence of kilometer-sized planetesimals at later ages.

Obtaining high signal-to-noise ground-based mid-infrared spectroscopy of debris disks has been challenging because typical debris disks have 10 μm fluxes, $F_\nu < 1$ Jy, making the majority of systems too faint to be studied spectroscopically from the ground and using *ISO*. The excellent sensitivity of the IRS (Houck et al. 2004) on *Spitzer* (Werner et al. 2004) has enabled the spectroscopic study of large samples of debris disks, including all objects discovered with the *IRAS* and *ISO* satellites. We present the first 5–40 μm spectroscopic study of a large sample of debris disks to study the growth of large bodies in circumstellar disks and to elucidate the physical processes acting on micron-sized grains.

Debris disks are dusty, gas-poor disks around main-sequence stars (Backman & Paresce 1993; Lagrange et al. 2000; Zuckerman 2001). Micron-sized dust grains are inferred to exist in these disks from measurements of their thermal emission at infrared through millimeter wavelengths. The estimated lifetimes for circumstellar dust grains due to radiation and corpuscular stellar wind pressure (if the grains are small), sublimation (if the grains are icy), Poynting-Robertson and corpuscular stellar wind drag, and collisions are typically significantly smaller than the estimated ages for the stellar systems, suggesting that the grains are replenished from a reservoir, such as sublimation of comets or collisions between parent bodies.

The dust grains observed around debris disks may be produced when planets gravitationally perturb parent bodies producing collisions. In our solar system, the zodiacal dust possesses dust bands that thermally emit $L_{\rm IR}/L_* = 10^{-7}$ times the incident stellar light and that have orbital properties identical to asteroid families, suggesting that the dust bands are generated by collisions between asteroids in each family. Gravitational perturbations by Jupiter and other planets in our solar system are expected to cause the apsides and nodes of asteroid orbits to precess at different rates because of small differences in their orbital parameters. This precession leads to asteroid collisions that generate the small grains observed in the dust bands. However, observed debris disks are typically 3–5 orders of magnitude more luminous than our zodiacal disk.

[1] Based on observations with the NASA *Spitzer Space Telescope*, which is operated by the California Institute of Technology for NASA.

[2] NOAO, 950 North Cherry Avenue, Tucson, AZ 85719; cchen@noao.edu.
[3] *Spitzer* Fellow.
[4] Department of Physics and Astronomy, University of Rochester, Rochester, NY 14627.
[5] Department of Physics, Ithaca College, Ithaca, NY 14850.
[6] Department of Physics and Astronomy, University of California, Los Angeles, CA 90095-1562.
[7] Center for Radiophysics and Space Research, Cornell University, Ithaca, NY 14853-6801.

Simulations of self-stirred disks suggest that the formation of icy planets, with radii 1000–3000 km, may trigger collisional cascades between the remaining nearby kilometer-sized planetesimals (Kenyon & Bromley 2004). Giant planet migration, soon after formation, may also trigger collisions. The migration of the Jovian planets in our solar system during the Late Heavy Bombardment may have caused gravitational resonances to sweep through the main asteroid belt, sending asteroids into the inner solar system, producing the craters observed on old terrestrial planet surfaces (Strom et al. 2005).

The presence of planets in debris disks may be inferred from the dynamical influence they exert on dust particles. Planets may produce central clearings in disks by gravitationally scattering dust grains out of the system that are otherwise spiraling toward their orbit center under Poynting-Robertson and corpuscular stellar wind drag and by trapping grains into mean motion resonances (Liou & Zook 1999; Quillen & Thorndike 2002). Unfortunately, directly resolving all but the nearest debris disks at infrared and submillimeter wavelengths, to search for disk structure generated by planets, is challenging with current ground- and space-based telescopes. However, the radial distribution of dust in a debris disk may be inferred from modeling the infrared spectral energy distribution (SED), assuming that the system is azimuthally symmetric.

Mid-infrared spectra of seven nearby debris disks, obtained with *Spitzer* IRS, have revealed that the majority of these systems do not possess spectral features, suggesting that the grains probably have $a > 10$ μm (Jura et al. 2004; Sloan et al. 2004). Jura et al. (2004) and Sloan et al. (2004) model the excess continua of these objects using a continuous disk with a uniform surface density, expected if Poynting-Robertson drag is the dominant dust removal mechanism, and using a single-temperature grain model. The disks around two-thirds of the stars in their sample appear to possess inner truncations at 10–50 AU. One possible explanation for the presence of central clearings is a planet at the truncation distance that sweeps the inner regions of the disk clear; however, central clearings may also be produced by sublimation if the grains are icy or by radiation pressure if the disks are collisionally dominated and grains with sub-blowout sizes are removed by radiation pressure. The SEDs of the remaining systems are consistent with a disk with a uniform surface density that may be produced when large grains, generated by collisions between parent bodies, spiral into their orbit center under the Poynting-Robertson effect (and stellar wind drag).

We report the results of a *Spitzer* IRS study of 59 main-sequence stars with published *IRAS* 60 μm excesses, building on initial results published by Jura et al. (2004). Jura et al. (2004) included LL spectra obtained for 19 debris disks. This study includes SL and LL or SH/LH data, depending on the *IRAS* 25 μm flux, and expands the target sample size. Refinements in the IRS flats have allowed us to improve the signal-to-noise at which the spectra are measured; therefore, we reanalyze objects in Jura et al. (2004) in addition to presenting new data. We list the targets for the full sample, along with their spectral types, distances, and published ages in Table 1.

2. SAMPLE SELECTION AND CHARACTERIZATION

The debris disks around Vega, Fomalhaut, ϵ Eridani, and β Pictoris were initially discovered from the presence of strong *IRAS* 60 and 100 μm excesses, 10–100 times larger than expected from the photosphere alone (Backman & Paresce 1993). Studies comparing the *IRAS* fluxes with predictions for the photospheric emission of field stars subsequently discovered more than 100 debris disk candidates, corresponding to a disk fraction ~15% (Backman & Paresce 1993; Coté 1987; Mannings & Barlow 1998; Sadakane & Nishida 1986; Sylvester et al. 1996; Walker & Wolstencroft 1988).

We selected 115 stars with *IRAS* 60 μm excesses, discovered in the studies listed above, for further study with the IRS. Approximately 25 of these targets are pre–main-sequence Herbig Ae/Be stars that will be discussed in L. Keller et al. (2006, in preparation), and another 30 of these targets are extended in the IRS slit, suggesting that the excess emission is generated by interstellar grains, as will be described in B. Sargent et al. (2006, in preparation). The discovery of extended infrared excess around two objects (HR 1307, HR 2522) is consistent with coronagraphic imaging that revealed the presence of reflection nebulosities in these systems (Kalas & Graham 2002). Modeling of the scattered light images suggest that the dust grains are small, interstellar grains, located at distances from 1000 to 100,000 AU, rather than large circumstellar grains at distances <100 AU from the central star (Kalas & Graham 2002).

We list the debris disks in our study with their stellar properties and reported *IRAS* 25, 60, and 100 μm excesses in Table 1. The majority of the stars in our sample are nearby (within 150 pc), isolated main-sequence stars, although a couple of objects may lie outside the local bubble and another nine objects are members of well-studied OB Associations or moving groups. For example, the star λ Cas is a member of Cas-Tau (de Zeeuw et al. 1999) with an estimated age of 10 Myr (Bhatt 2000). The star HD 146897 is a member of Upper Scorpius and the stars HD 95086, G Cen, HD 110058, and HD 113766 are members of Lower Centaurus Crux in Sco-Cen (de Zeeuw et al. 1999) with estimated ages of 5 and 16 Myr (Mamajek et al. 2002), respectively. The stars HR 7012, η Tel, and HD 181327 are members of the β Pic moving group with estimated ages of ~12 Myr (Zuckerman et al. 2001).

Since we would like to study the evolution of dust properties as a function of time, we estimate ages for as many stars in the sample as possible by fitting log g and $T_{\rm eff}$ to Schaller et al. (1992) isochrones for B-, A-, and F-type stars. We estimate log g and $T_{\rm eff}$ (see Table 1) from mean General Catalogue of Photometic Data Strömgren photometry (Mermilliod et al. 1997) using the calibration of Napiwotzki et al. (1993) and the rotation correction of Figueras & Blasi (1998). B-, A-, and F-type stars that appear above the published isochrones are assigned ages of 1, 50, and 300 Myr, respectively, the ages for which the main-sequence isochrones begin. We estimate uncertainties in our estimated ages of a factor of 2. For comparison, we also list published isochronal and moving group ages in Table 1. For cases in which the moving group age is inconsistent with the isochronal age, we assume that the moving group ages are more accurate because stars above the zero-age main sequence in the HR diagram may be either evolving down onto the main sequence or up and away from the main sequence.

3. OBSERVATIONS

We obtained IRS spectra of 59 main-sequence stars with previously reported *IRAS* 60 μm excesses (Backman & Paresce 1993; Coté 1987; Mannings & Barlow 1998; Sadakane & Nishida 1986; Sylvester et al. 1996; Walker & Wolstencroft 1988) with either (1) both the Short-Low (5.2-14.0 μm) and Long-Low (14.0–38.0 μm; $\lambda/\Delta\lambda \sim 90$) modules or (2) the Short-Low, Short-High (9.9–19.6 μm), and Long-High (18.7–37.2 μm; $\lambda/\Delta\lambda \sim 600$) modules. In order to avoid time-consuming peak-up on our relatively bright targets with accurately known positions, we operated the observatory in IRS spectral mapping mode where a 2×3 raster (spatial times dispersion) centered on the star is performed (Watson et al. 2004). We carried out the

TABLE 1

Stellar Properties

HR	HD	Name	Spectral Type	Distance (pc)	$v \sin i$ (km s^{-1})	A_V (mag)	T_{eff} (K)	log g	Age (This Work) (Gyr)	Age (Literature) (Gyr)	25 μm Excess (Jy)	60 μm Excess (Jy)	100 μm Excess (Jy)	Excess Reference
123..........	2772	λ Cas†	B8 Vn	109	220	0.03	13290	3.946	0.11	0.01[a]	0.00	0.96	2.44	1
333..........	6798		A3 V	83	190	0.00	10360	4.243	0.11	...	0.00	0.34	0.00	1
451..........	9672	49 Cet	A1 V	61	195	0.00	9970	4.369	0.05	0.02[b]	0.33	1.99	1.90	1, 3, 4, 6
493..........	10476	107 Psc	K1 V	7	10	0.00	5390	4.878	...	...	0.10	0.11	0.38	1
506..........	10647		F9 V	17	5	0.00	6260	4.598	0.3	0.3, 4.8[b,c]	0.14	0.81	0.00	1, 3
509..........	10700	τ Cet	G8 V	4	7	0.00	6000	5.288	...	7.2[d]	0.06	0.08	0.42	1, 3
664..........	14055	γ Tri	A1 Vnn	36	230	0.00	10540	4.172	0.17	0.16[b]	0.21	0.81	0.83	1
	16157	CC Eri	M0	12	...	0.00	3900	...	...	...	0.16	0.10	0.21	3
818..........	17206	τ^1 Eri	F5/F6 V	14	25	0.00	6480	4.500	0.3	3.5[c]	0.17	0.89	3.65	1
919..........	18978	τ^3 Eri	A4 V	26	120	0.00	8610	4.110	0.5	...	0.02	0.04	0.15	1
963..........	20010	α For	F8 IV	14	15	0.00	6360	4.169	2.7	4.3[c]	−0.02	0.11	0.00	1, 6
1082..........	21997		A3 IV/V	74	60	0.00	9000	4.349	0.15	0.1[b]	0.00	0.58	0.00	1
1338..........	27290	γ Dor	F4 III	20	65	0.00	7290	4.260	0.40	...	0.05	0.21	0.21	1, 3, 6
1570†........	31295		A0 V	37	110	0.43	9450	4.212	0.23	0.01, 0.1[b,e]	0.00	0.42	0.00	1, 4
1686†........	33564		F6 V	21	10	0.00	6430	4.238	2.0	3.0[c]	−0.04	0.23	0.00	1
1705..........	33949	κ Lep†	B7 V	172	125	0.00	12740	3.497	0.12	...	0.13	0.41	...	3, 4
1839..........	36267	32 Ori†	B5 V	89	190	0.00	16430	4.441	0.001	...	0.00	0.55	0.00	1
1998..........	38678	ζ Lep	A2 Vann	22	245	0.00	9910	4.213	0.18	0.23[f]	0.68	0.40	<0.11	1, 2, 3
2015..........	39014	δ Dor	A7 V	44	170	0.00	8360	3.734	0.59	0.49, 0.54[e,f]	0.04	0.45	1.11	1, 2
2124†........	40932		A2 V	47	18	0.47	8350	3.969	0.67	0.69[f]	0.63	3.20	2.75	1
2161..........	41814	XZ Lep	B3 V	496	35	0.12	17890	4.197	0.017	...	0.00	0.57	0.00	1
2483..........	48682	ψ5 Aur†	G0 V	17	5	0.00	6350	4.608	...	4.5[c]	0.11	0.43	0.53	1
	53143		K1 V	18	4	0.00	5000	...	...	0.3, 0.97[b,g]	0.02	0.14	0.66	3
3220..........	68456		F5 V	21	15	0.00	6600	4.259	1.7	2.6[c]	0.04	1.76	3.05	1
3314..........	71155		A0 V	38	120	0.00	10190	4.190	0.19	0.17, 0.24[e,f]	−0.03	0.57	...	2
3485..........	74956	δ Vel	A1 V	24	150	0.00	9820	3.904	0.35	0.39[f]	0.03	0.29	<0.02	1, 2, 6
...	FI Vir		M4	3	...	0.00	3400	...	...	...	...	0.12	0.22	1
3862..........	84117		G0 V	15	6	0.00	6290	4.338	1.9	4.6[c]	0.12	0.13	0.24	1
3927..........	86087		A0 V	98	...	0.00	10090	4.400	0.05	...	0.00	0.68	0.00	1
	95086		A8 III	92	...	0.00	7500	...	...	0.016[a]	<0.25	0.60	<0.80	3
4295..........	95418	β UMa	A1 V	24	32	0.00	9790	3.881	0.34	0.36[f]	0.24	0.43	0.00	1, 2
4534..........	102647	β Leo	A3 V	11	110	0.00	9020	4.293	0.05	0.05[f]	0.41	0.77	0.63	1, 2, 6
4732..........	108257	G Cen†	B3 Vn	123	245	0.16	17930	4.140	0.025	0.016[a]	0.44	0.88	0.00	1
4775..........	109085	η Crv	F2 V	18	92	0.00	6890	4.28	...	1.0[h]	2.24	0.77	0.31	3, 5
	110058		A0 V	100	...	0.40	9500	...	...	0.016[a]	0.30	0.51	<1.00	3
	113766†		F3/F5 V	131	...	0.05	6870	4.360	...	0.016[a]	1.80	0.65	<1.00	3
5236..........	121384		G6 IV–V	38	...	0.00	5670	5.070	...	4.1[c]	0.00	0.34	<10.2	6
5351..........	125162	λ Boo	A0p	30	110	0.00	9310	4.193	0.27	0.18, 0.31[e,f]	0.09	0.45	...	4
5447..........	128167	σ Boo	F2 V	15	10	0.00	6830	4.408	1.4	1.0, 1.7[b,c,d]	0.06	0.09	<0.06	1
5671..........	135382	γ Tra	A1 V	56	200	0.03	10060	3.244	0.17	0.26[e]	0.06	0.07	1.51	2
5793..........	139006	α CrB	A0 V	23	132	0.00	10180	3.949	0.30	0.31[f]	0.31	0.50	0.00	1, 2
	139664		F5 IV–V	18	87	0.02	6900	4.450	0.48	0.2, 1.1, 1.6[b,c,d]	0.33	0.54	<2.35	6
5933..........	142860	41 Ser	F6 IV	11	10	0.00	6430	4.348	1.6	3.2, 3.3[c,d]	−0.08	0.24	0.00	1
	146897		F2/F3 V	132	...	0.31	6750	...	...	0.005[a]	<0.6	0.73	<3.05	
6168..........	149630	σ Her	B9 V	93	285	0.00	11440	3.685	0.17	0.23[i]	0.02	0.22	0.00	1, 2, 4
6297..........	153053		A5 IV–V	51	...	0.22	8070	4.030	0.42	...	1.03	1.81	...	2
6486..........	157792		A3m...	26	68	0.00	7660	4.222	0.24	0.74[d]	0.15	1.02	11.48	1
6532†........	159082		B9	152	20	0.25	11210	4.019	0.2	...	0.00	0.69	1.28	1
6533..........	159139	78 Her	A1 V	84	260	0.00	10980	4.305	0.05	...	0.00	0.46	1.23	1
6585..........	160691	μ Ara	G3 IV–V	15	...	0.00	5500	...	...	6.2[d]	0.22	0.08	<0.96	1
6629..........	161868	γ Oph	A0 V	29	212	0.00	10200	4.189	0.19	0.18[f]	0.17	1.23	0.00	1, 2, 4
6670..........	162917		F4 IV–V	31	20	0.00	6670	4.369	1.6	1.4[c]	<0.09	0.52	...	4
7012..........	172555		A5 IV–V	29	175	0.00	8550	4.377	0.05	0.012[j]	0.61	1.92	...	2

TABLE 1—*Continued*

HR	HD	Name	Spectral Type	Distance (pc)	$v \sin i$ (km s^{-1})	A_V (mag)	$T_{\rm eff}$ (K)	log g	Age (This Work) (Gyr)	Age (Literature) (Gyr)	25 μm Excess (Jy)	60 μm Excess (Jy)	100 μm Excess (Jy)	Excess Reference
7329..........	181296	η Tel†	A0 Vn	48	420	0.12	10180	4.893	0.05	0.012[j]	0.35	0.51	0.00	1, 3
	181327		F5/F6 V	51	...	0.00	6560	4.510	1.4	0.012, 1.3[c,j]	0.20	2.00	1.90	3
	191089		F5 V	54	...	0.00	6540	4.420	1.6	<0.1, 3.0[b,c]	0.34	0.71	0.33	3
	200800		A3 Vm	127	...	0.09	8650	...	...	...	0.31	0.15	0.34	3
8799..........	218396		A5 V	40	40	0.34	7410	4.163	0.59	0.03, 0.73[b,f]	<0.19	0.45	...	4
	221354		K2 V	17	...	0.00	5350	4.270	...	1.5[g]	0.09	0.88	<20.5	6

NOTE.—Dagger (†) signifies a binary system.
[a] de Zeeuw et al. (1999).
[b] Zuckerman & Song (2004).
[c] Nordstrom et al. (2004).
[d] Lachaume et al. (1999).
[e] Paunzen (1997).
[f] Song et al (2001).
[g] Song et al. (2000).
[h] Wyatt et al. (2005).
[i] Grosbol (1978).
[j] Zuckerman et al. (2001).
REFERENCES.—(1) Backman & Paresce 1993; (2) Coté 1987; (3) Mannings & Barlow 1998; (4) Sadakane & Nishida 1986; (5) Sylvester et al. 1996; (6) Walker & Wolstencroft 1988.

bulk of the reduction and analysis of our spectra with the IRS team's SMART program (Higdon et al. 2004).

We estimate the stellar photospheric fluxes of our objects by minimum χ^2 fitting published photometry from the literature to model stellar atmospheres, using only bandpasses with wavelengths shorter than 3 μm: TD 1 (Thompson et al. 1978), Johnson et al. (1966), and 2MASS (Cutri et al. 2003). For stars with spectral types earlier than K2 V, we use 1993 Kurucz stellar atmospheres; for stars later than K2 V, we use Nextgen models. We assume that all stars have solar abundances and log $g = 4.5$ unless otherwise noted. We use the Cardelli et al. (1989) extinction law to estimate $E(B-V)$ and list the extinctions $[A_V = 3.1E(B-V)]$ estimated from photosphere fitting in Table 1. We plot the SEDs for all of our objects in Figure 1. Ultraviolet through near-infrared photometry is shown with black symbols; IRS spectra are shown in red; Multiband Imaging Photometer for *Spitzer* (MIPS) photometry, where available (Bryden et al. 2006; Rieke et al. 2005), are shown with blue error bars; *IRAS* photometry is shown with green error bars and upper limit symbols; and submillimeter photometry, where available (Wyatt et al. 2005; Greaves et al. 2004; Sheret et al. 2003; Holmes et al. 2003), is shown with black error bars and upper limit symbols. Our photosphere models are shown with a solid black line.

We measure the flux of our objects in two photometric bands to search for excess emission from silicates (8.5–13 μm) and cold grains (30–34 μm). The calibration uncertainty in the fluxes is ~5% and the measured statistical uncertainties are listed in Table 2. We find 25 sources without strong IRS excesses despite reported *IRAS* 60 μm excesses (annotated in Table 2). The average fractional excess, $[F_\nu(\text{measured}) - F_\nu(\text{predicted})]/F_\nu(\text{predicted})$, for these photospheric objects is slightly negative in the 8.5–13 μm band (-0.028 ± 0.055) with a standard deviation consistent with IRS observations of nearby, solar-like stars (Beichman et al. 2006). The average fractional excess is slightly higher in the 30–34 μm band and possesses a larger standard deviation (0.08 ± 0.13), indicating that some of these sources may possess weak excesses at the longest IRS wavelengths. For sources that are not saturated and do not possess excess in the 8.5–13 μm band, we also normalized the photosphere to the first 10 data points in the SL module to search more sensitively for excesses in the 30–34 μm band. Values of this calibration factor deviated from unity on a star-by-star basis by less than 5%. Pinning the photosphere to the fluxes at the shortest wavelengths of the SL module produces average fractional excesses for the 25 stars without IRS excesses of -0.032 ± 0.048 and 0.06 ± 0.13 at 8.5–13 and 30–34 μm, respectively. In our analysis, we use photosphere models that are scaled to the first 10 points of SL unless the source is saturated or possesses a 8.5–13 μm excess.

The significantly larger *IRAS* beam may contain multiple sources and therefore be responsible for some of the discrepancy between the *IRAS* and *Spitzer* IRS results. For reference, the *IRAS* beam is $1' \times 5'$ at 12 and 25 μm, $2' \times 5'$ at 60 μm, and $4' \times 5'$ at 100 μm. By contrast, point sources observed with *Spitzer* MIPS have an FWHM of ~6″ at 24 μm and an FWHM of ~20″ at 70 μm. The color-corrected *IRAS* 25 μm fluxes are significantly higher than the IRS 25 μm fluxes for three objects (HR 2124, HR 6297, and HD 200800). HR 6297 has been observed with MIPS at 24 μm. In this case, the discrepancy between the HR 6297 *IRAS* and IRS fluxes can definitely be explained by the presence of a second source in the *IRAS* beam. The *IRAS* Point Source Catalog 25 μm flux for HR 6297 is (not color-corrected) ~410 mJy (with a central position 0.′4 away from the star), while the IRS 25 μm flux is ~90 mJy. MIPS 24 μm images reveal two sources near HR 6297: one at the position of HR 6297 with $F_\nu(23.68\ \mu\text{m}) =$ 82 mJy, consistent with the IRS spectrum, and another, brighter source 0.′92 west of HR 6297 with $F_\nu(23.68\ \mu\text{m}) = 207$ mJy. The *IRAS* PSC flux is the sum of the two MIPS sources and is therefore an overestimate of the HR 6297 25 μm flux. Unfortunately, the remaining two sources with possibly confused *IRAS* 25 μm fluxes have not been observed with MIPS. We searched the 2MASS catalog around the positions of HR 2124 and HD 200800 for additional sources of confusion. For comparison, we examined the 2MASS colors for the unexpected 25 μm source (located at $17^{\rm h}00^{\rm m}00\overset{\rm s}{.}07$, $-54°35'38\overset{''}{.}6$ [J2000.0]) in the HR 6297 *IRAS* beam (the spurious source possesses $J = 6.69$, $H =$ 5.73, and $K = 5.38$). We found a bright source with similarly red 2MASS colors, 0.′9 away from HD 200800 (located at $21^{\rm h}09^{\rm m}13\overset{\rm s}{.}83$, $-65°47'38\overset{''}{.}4$ [J2000.0]) with $J = 6.40$, $H = 5.47$, and $K = 5.17$. However, we were not able to find an obvious candidate for the extra emission in the *IRAS* HR 2124 beam. There

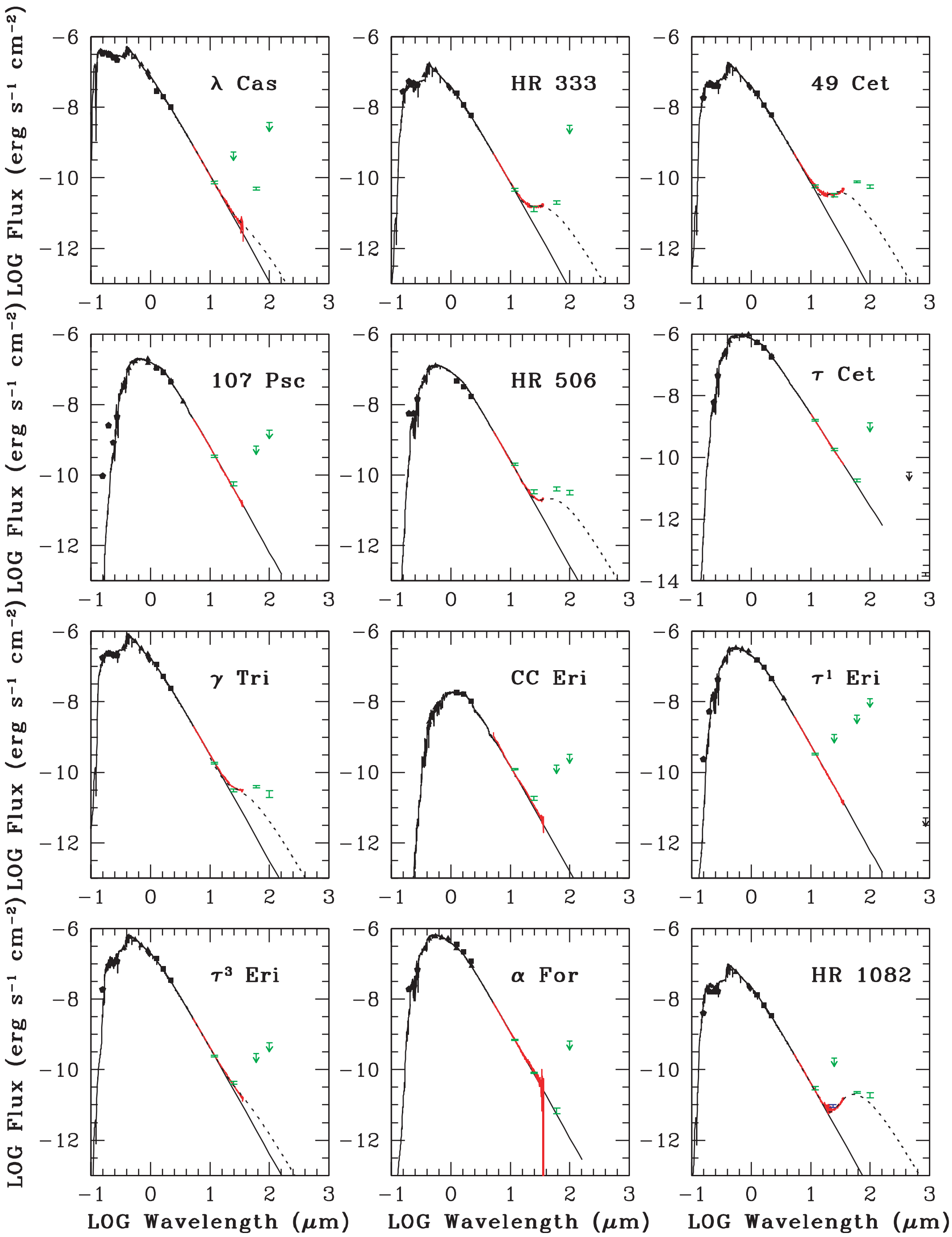

Fig. 1.—Spectral energy distributions (SEDs) for all objects in our sample. TD1 fluxes (Thompson et al. 1978) are plotted as pentagons; General Catalogue of Photometric Data mean *UBV* or Johnson et al. (1966) fluxes are plotted as triangles; and 2MASS *JHK* fluxes (Cutri et al. 2003) are plotted as squares. Color-corrected *IRAS*, MIPS, and submillimeter photometry, where available, are shown with green, blue, and black error bars and upper limit symbols, respectively. Our *Spitzer* IRS spectra, as reported here, are shown in red. Overlaid are the best-fit 1993 Kurucz and Nextgen models for the stellar atmospheres.

are 7 2MASS sources within 2′ of HR 2124 with $J - K > 1$, but all have $K \sim 14$–15, suggesting that they are probably too faint to be detected at 24 μm despite their red colors.

The presence of *IRAS* 60 μm excess does not necessarily imply the presence of 5–35 μm excess. Twenty−five objects in our sample (∼42%) do not possess strong infrared excess at 5–35 μm despite the identification of *IRAS* excess in the literature. The discrepancy between published *IRAS* results and our results may (1) reflect difficulties in either the search criteria or the data reduction in the original searches, (2) be due to the presence of cold dust that is not detected at IRS wavelengths, or (3) be due to source confusion in the *IRAS* beam. Eleven of the objects in our study possess *IRAS* 12 and 25 μm fluxes that are consistent with our photosphere models and *IRAS* upper limits or photosphere detections in the *IRAS* Point Source or Faint Source Catalogs at $\lambda \geq 60$ μm (107 Psc, CC Eri, τ^1 Eri, α For, HR 1686, δ Dor, HR 3220, FI Vir, HR 3862, G Cen, and μ Ara) despite reports of measured excess in the literature. The discprepancy in these cases may be due to difficulties in the search criteria or data reduction. Our sample is drawn from several *IRAS* searches for debris disks

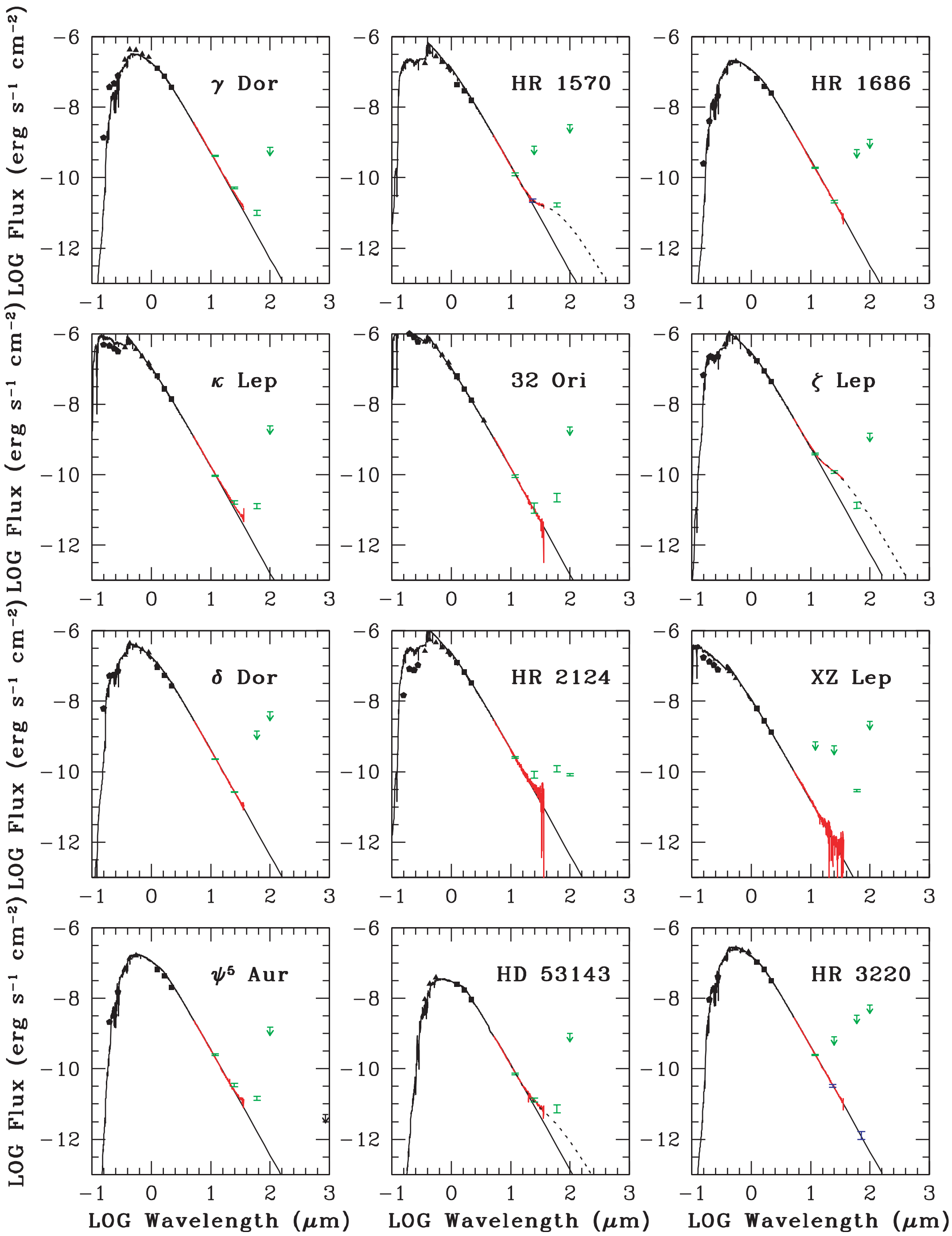

FIG. 1.—*Continued*

that used different criteria to establish whether a source possessed an infrared excess. Coté (1987) selected sources with $V-[12]$, $V-[25]$, $V-[60] > 0.5$; Sadakane & Nishida (1986) selected sources with $[12]-[60] > 1$; and Walker & Wolstencroft (1988) selected sources with $F_\nu(60\ \mu\mathrm{m})/F_\nu(100\ \mu\mathrm{m}) = 0.8$–$2.0$, similar to that observed toward β Pic, Vega, Fomalhaut, and ϵ Eridani.

The dust in many of the undetected systems may be cold. The IRS spectra for five objects are photospheric over the bulk of the IRS wavelength range but may be rising at $\lambda \sim 35\ \mu$m, although with insufficient signal–to-noise to model these systems in detail (κ Lep, HR 2124, XZ Lep, γ Tra, and HD 200800). The dust in some systems may be so cold that excess emission cannot be easily detected above the photosphere at IRS wavelengths. Ten sources possess *IRAS* 60 μm flux excesses but no evidence for significant IRS excess at $\lambda < 35\ \mu$m (τ Cet, γ Dor, 32 Ori, ψ^5 Aur, δ Vel, HR 5236, σ Boo, 41 Ser, σ Her, and HD 221354). If the dust in these systems has $T_{\rm dust} < 60$ K, then the infrared excess at the longest IRS wavelengths could be small and changing slowly compared to the stellar photosphere, making the excess difficult to infer. For τ Cet, our measured and predicted fluxes, $F_\nu(8.5$–$13\ \mu\mathrm{m}) = 7470$ and 7710 mJy, respectively, and $F_\nu(30$–$34\ \mu\mathrm{m}) = 786$ and 829 mJy, respectively, suggesting that this source possesses -3% and -5% excesses at 8.5–13 and 30–34 μm, respectively. However, the 60–850 μm excesses observed

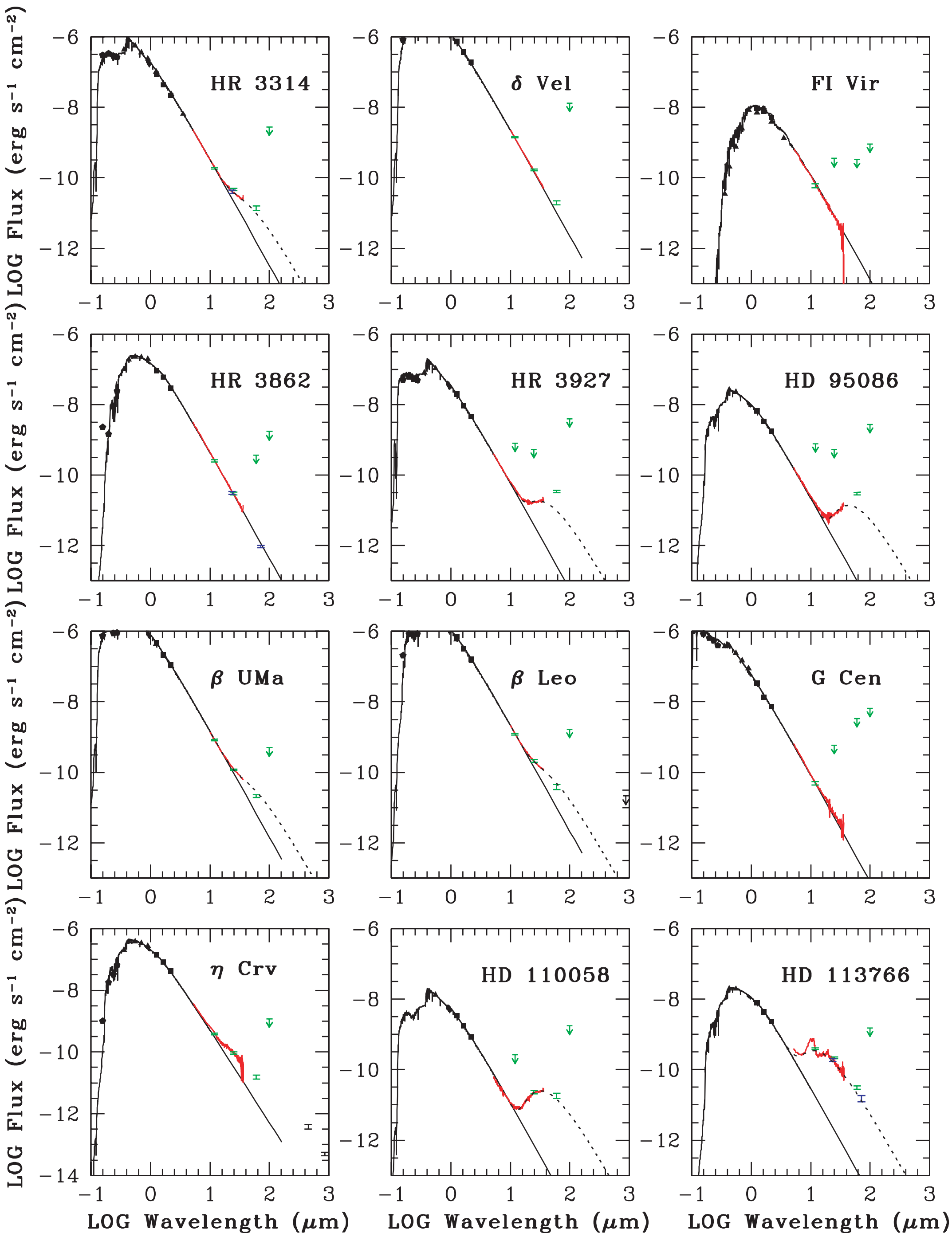

Fig. 1.—*Continued*

toward τ Cet are easier to detect because the photosphere is negligible at these wavelengths; these excesses are fitted by a modified 60 K blackbody (Greaves et al. 2004), implying that the slope of the 20–35 μm spectrum should be ~4% higher than without the excess. Alternately, the *IRAS* flux for some objects may include extragalactic or other stellar sources that were included in the large *IRAS* beam.

4. GRAIN COMPOSITION

Five objects in our sample possess 10 and/or 20 μm spectral features: HR 3927, η Crv, HD 113766, HR 7012, and η Tel (see Fig. 2). We model the excess emission for these objects assuming that the observed features are generated by amorphous olivine and pyroxene, and crystalline forsterite, enstatite, and silica. We model the remaining continuum emission using amorphous carbon and one (or two) blackbody distributions. We do not observe PAH emission features toward any of the objects in our sample.

A lower limit to the size of dust grains orbiting a star can be found by balancing the force due to radiation pressure with the force due to gravity. For small grains with radius a, the force due to radiation pressure overcomes gravity for solid particles larger than

$$a_{\mathrm{min},0} = 3L_* Q_{\mathrm{pr}}/(16\pi G M_* c \rho_s) \tag{1}$$

(Artymowicz 1988), where L_* and M_* are the stellar luminosity and mass, Q_{pr} is the radiation pressure coupling coefficient, and

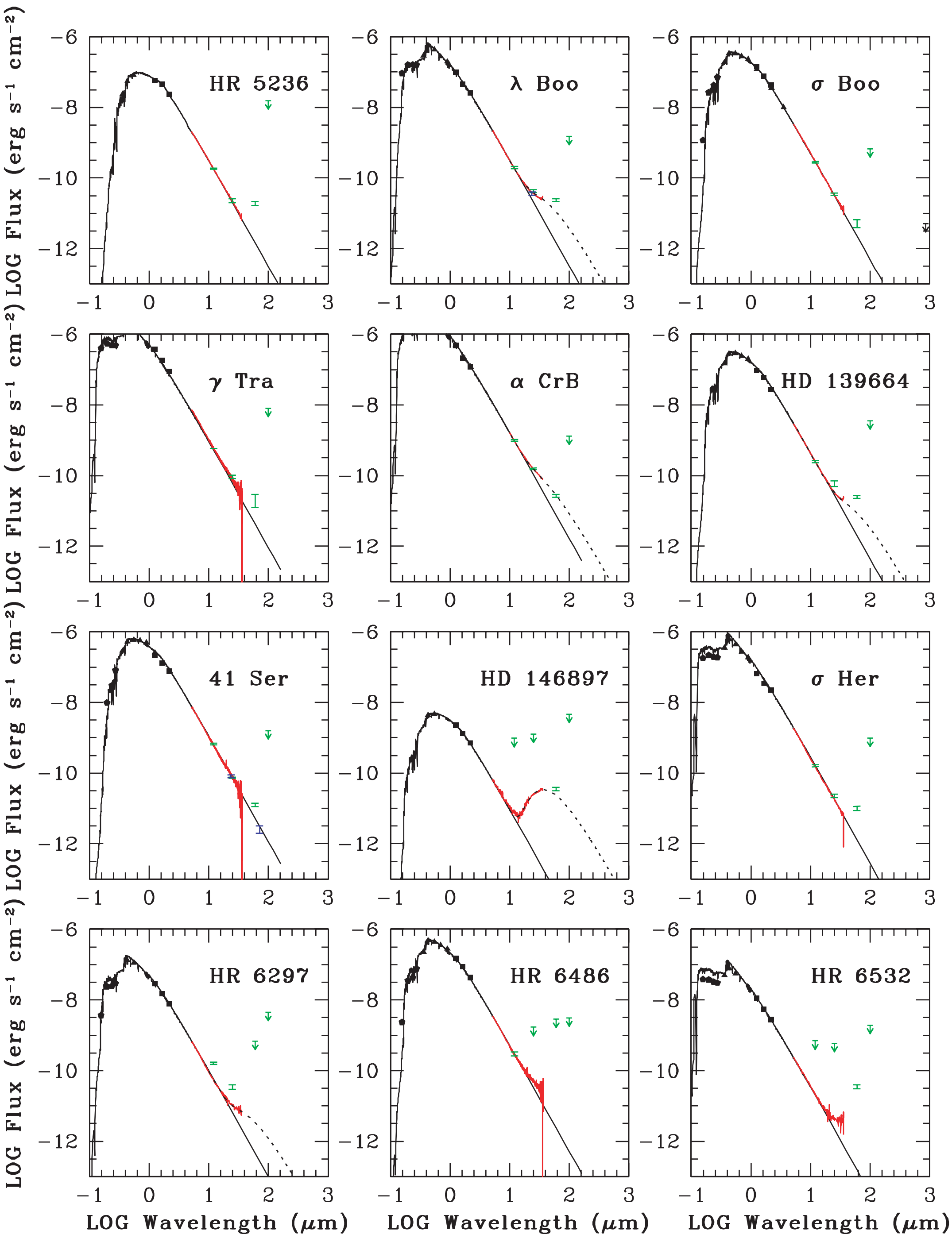

FIG. 1.—*Continued*

ρ_s is the density of an individual grain. We assume that the bulk density of silicate, amorphous carbon, and silica grains are $\rho_s =$ 3.3, 2.5, and 2.3 g cm^{-3}, respectively. Since radiation from A−type (HR 3927, HR 7012, and η Tel) and F-type (η Crv and HD 113766) stars is dominated by optical and ultraviolet light, we expect that $2\pi a/\lambda \gg 1$ and therefore the effective cross section of the grains can be approximated by their geometric cross section so $Q_{pr} \approx 1$. We estimate the stellar mass by fitting our inferred T_{eff} and log g to the Schaller et al. (1992) isochrones for A-type stars and by fitting our inferred T_{eff} and L_* to Siess et al. (2000) isochrones for F-type stars. We list the minimum grain sizes, $a_{min,0}$, for solid silicate, amorphous carbon, and silica grains around each object if the species is required in the fit in Table 3. If the grains are porous (with a volume fraction, $f = V_{vac}/V_{tot} > 0$), then the minimum-sized grains estimated in equation (1) must be modified to account for the vacuum fraction:

$$a_{min}(f) = \frac{a_{min,0}}{1-f}. \quad (2)$$

In fitting the 5–40 μm spectra of HR 3927, η Crv, HD 113766, HR 7012, and η Tel, we assume that the grains are spheres with radius $a > a_{min}$. We list the solid angles subtended by each dust population Ω, their mass m and temperature, the radii of each grain population, and its vacuum volume fraction in Table 3. We infer absorption coefficients, $Q_{abs}(\lambda)$, using optical constants

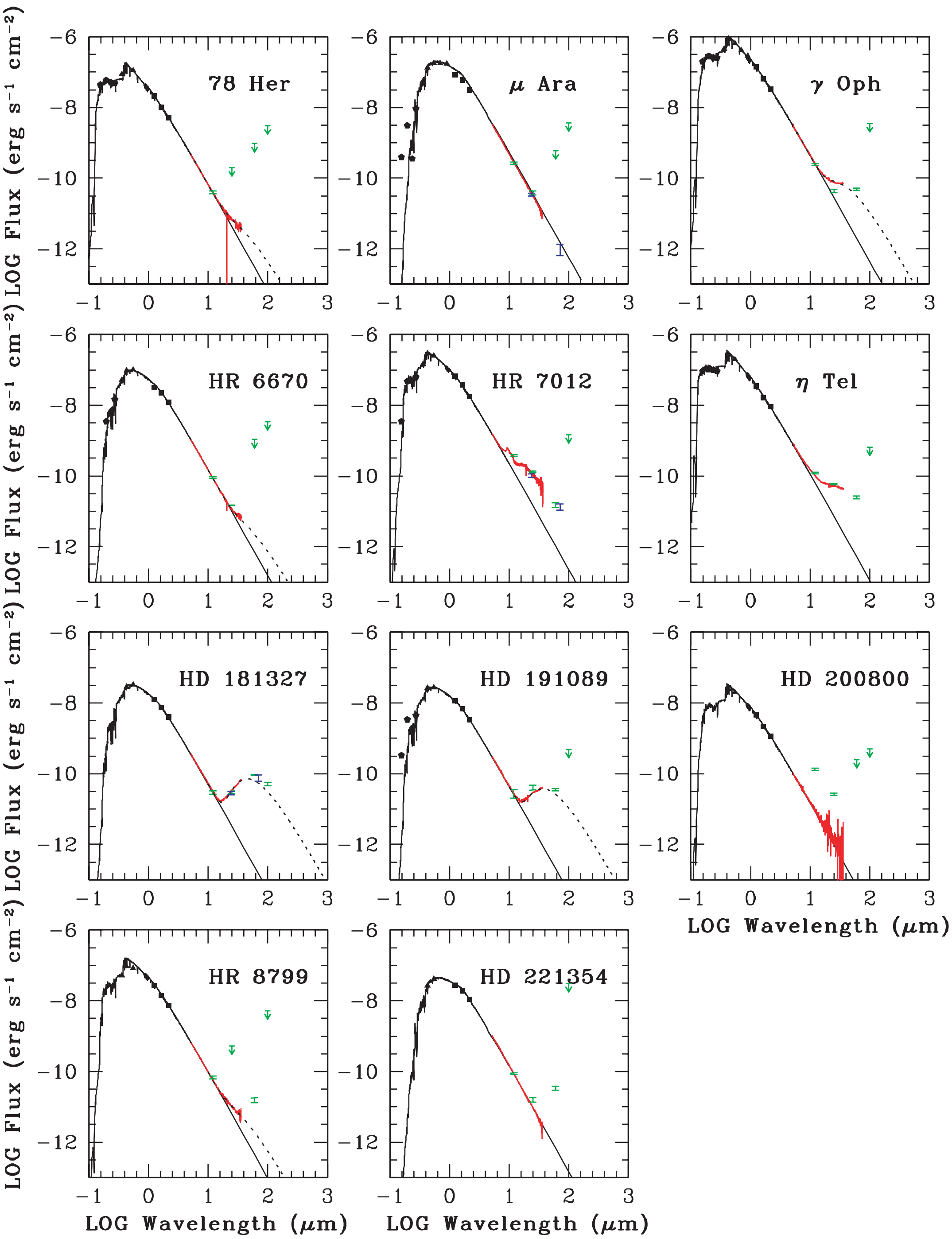

Fig. 1.—*Continued*

published in the literature for amorphous olivine ($MgFeSiO_4$; Dorschner et al. 1995), amorphous pyroxene ($Mg_{0.5}Fe_{0.5}SiO_3$ and $Mg_{0.8}Fe_{0.2}SiO_3$; Dorschner et al. 1995), crystalline forsterite ($Mg_{1.9}Fe_{0.1}SiO_4$; Fabian et al. 2001), crystalline enstatite ($MgSiO_3$; Jaeger et al. 1998), and amorphous carbon (Zubko et al. 1996), and Bruggeman Effective Medium Theory (Bohren & Huffman 1983). (Please see Sargent et al. 2006 for a more detailed description of $Q_{abs}(\lambda)$ estimates.) Nonzero vacuum volume fractions shift the peak positions of silicate features to longer wavelengths and broaden the features (Kessler-Silacci et al. 2006).

Our fits to the HD 113766 and HR 7012 spectra require the presence of small sub-micron–sized grains (crystalline enstatite, silica, and amorphous carbon). In these cases, we modeled the submicron dust components using laboratory measured opacities of crushed forsterite (Mg_2SiO_4; Koike et al. 2003) and enstatite ($Mg_{0.7}Fe_{0.3}SiO_4$; Chihara et al. 2002) and optical constants for silica (cristobalite; Simon & McMahon 1953) assuming that the distribution of grain shapes is well-described by the continuous distribution of ellipsoids (CDE; Fabian et al. 2001). Both of these systems are young with estimated ages ~16 and ~12 Myr, respectively. The disks around both stars are optically thin and possess high fractional infrared luminosities, $L_{IR}/L_* = 0.015$ and 10^{-3}, respectively. Since the estimate ages of these systems are ~16 and ~12 Myr, based on their membership in Lower Centaurus Crux in Sco-Cen and the β Pictoris Moving Group, these systems probably no longer contain bulk molecular gas. Therefore, we hypothesize

TABLE 2

IRS Photometry in 8.5–13 and 30–34 μm Bands

	8.5–13 μm				30–34 μm				
Name	Measured Flux (mJy)	Predicted Flux (mJy)	Excess (mJy)	Fractional Excess (mJy)	Measured Flux (mJy)	Predicted Flux (mJy)	Excess (mJy)	Fractional Excess (mJy)	*Spitzer* AOR Key
λ Cas	341 ± 0.8	350	−9.3	−0.027	55.9 ± 1.4	37.5	19.2	0.524	3575040
HR 333	227 ± 0.3	212	14.7	0.069	161 ± 2	23.4	138	6.14	3553536
49 Cet	270 ± 0.6	218	52.7	0.242	426 ± 1	23.9	402	16.8	4928768
107 Psc‡	1860 ± 0.5	1880	−29.1	−0.015	201 ± 1	196	−5.3	−0.026	3554048
HR 506	747 ± 0.9	773	−26.4	−0.034	197 ± 2	84.4	114	1.36	3553792
τ Cet‡	7470 ± 10	7710	−237	−0.031	786 ± 3	829	−42.8	−0.052	4932352
γ Tri	951 ± 1	923	27.4	0.030	327 ± 2	97.1	229	2.34	3554304
CC Eri‡	439 ± 0.6	558	−119	−0.213	55.6 ± 1.1	59.9	−5.7	−0.093	3554560
τ^1 Eri‡	1740 ± 2	1780	−40.3	−0.023	186 ± 2	199	−4.9	−0.026	3554816
τ^3 Eri	1270 ± 1	1250	29.3	0.024	196 ± 1	132	63.3	0.477	4931840
α For‡	3410 ± 4	3450	−38.7	−0.011	413 ± 5	378	28.3	0.074	3555072
HR 1082	125 ± 0.3	123	1.7	0.014	117 ± 2	12.9	104	7.96	3555328
γ Dor‡	1540 ± 2	1580	−36.2	−0.023	194 ± 2	170	24.8	0.147	3555584
HR 1570	635 ± 0.9	663	−29.4	−0.044	175 ± 2	69.0	105	1.50	3555840
HR 1686‡	889 ± 1	936	−46.9	−0.050	106 ± 2	101	6.1	0.061	3556096
κ Lep‡	521 ± 0.6	517	4.1	0.008	73.1 ± 1.3	53.1	19.2	0.356	3577600
32 Ori‡	468 ± 0.5	492	−23.6	−0.048	50.4 ± 1.7	47.1	−0.6	−0.012	3556352
ζ Lep	1950 ± 0.6	1710	232	0.136	886 ± 4	182	704	3.87	4932864
δ Dor‡	1210 ± 1	1240	−33.1	−0.027	135 ± 2	131	3.2	0.024	3556608
HR 2124‡	1260 ± 2	1350	−95.1	−0.070	203 ± 5	144	54.2	0.365	3556864
XZ Lep‡	48.1 ± 0.3	45.3	2.7	0.061	5.5 ± 2.1	4.6	0.8	0.168	3585536
ψ^5 Aur‡	1010 ± 1	1045	−35.8	−0.034	140 ± 2	111	28.4	0.255	3557120
HD 53143	380 ± 0.4	395	−14.6	−0.037	82.0 ± 1.1	41.6	39.3	0.919	3557632
HR 3220‡	1260 ± 2	1260	−7.1	−0.006	143 ± 2	137	7.7	0.057	3557888
HR 3314	987 ± 0.8	978	9.5	0.010	281 ± 2	103	177	1.71	3558144
δ Vel‡	6850 ± 7	6810	35.1	0.005	766 ± 4	721	44.6	0.062	4930816
FI Vir‡	343 ± 0.4	348	−5.6	−0.016	37.5 ± 1.4	41.5	−2.2	−0.054	3559168
HR 3862‡	1310 ± 1	1370	−66.0	−0.048	140 ± 2	146	−7.1	−0.048	3558400
HR 3927	195 ± 0.4	177	18.1	0.102	187 ± 2	18.8	168	8.94	3558656
HD 95086	75.3 ± 0.3	69.0	12.5	0.199	114 ± 2	7.6	107	14.6	3558912
β UMa	4110 ± 5	4160	−48.8	−0.012	801 ± 3	440	361	0.820	4930304
β Leo	6390 ± 7	6370	18.3	0.003	1410 ± 6	676	736	1.09	4929793
G Cen‡	259 ± 0.5	268	−7.9	−0.029	34.7 ± 2.2	27.3	7.1	0.269	3579392
η Crv	1890 ± 3	1610	276	0.171	476 ± 1	179	197	1.10	3559424
HD 110058	55.3 ± 0.3	40.3	15.0	0.372	380 ± 2	4.3	376	88.1	3579648
HD 113766	1870 ± 2	86.2	1780	20.650	988 ± 4	9.6	978	102	3579904
HR 5236‡	931 ± 0.5	901	28.9	0.032	105 ± 0.9	96.1	7.6	0.078	3559680
λ Boo	936 ± 0.9	937	−0.5	−0.001	272 ± 2	100	173	1.75	3559936
σ Boo‡	1510 ± 1	1540	−29.8	−0.019	172 ± 2	164	7.4	0.045	3560192
γ Tra‡	3090 ± 2	3190	−99.8	−0.031	359 ± 5	345	9.2	0.026	3560448
α CrB	4860 ± 2	4830	30.0	0.006	988 ± 4	511	476	0.932	4929280
HD 139664	1260 ± 1	1250	7.7	0.006	223 ± 2	135	89.2	0.666	3560704
41 Ser‡	3160 ± 3	3320	−159	−0.048	364 ± 4	368	−5.4	−0.015	3561216
HD 146897	34.7 ± 0.3	27.0	7.6	0.283	329 ± 3	2.9	327	113	3581696
σ Her‡	750 ± 0.8	797	−46.9	−0.059	87.0 ± 3.5	85.2	2.9	0.034	3561472
HR 6297	271 ± 0.3	287	−16.8	−0.058	80.4 ± 2.2	31.1	49.9	1.64	3561728
HR 6486	1470 ± 2	1520	−59.9	−0.039	310 ± 5	168	142	0.846	3562240
HR 6532	106 ± 0.3	102	4.0	0.039	40.2 ± 2.0	10.5	29.4	2.74	3582720
78 Her	208 ± 0.4	208	0.9	0.004	47.9 ± 12.7	21.9	25.9	1.18	3562496
μ Ara‡	1400 ± 1	1490	−91.2	−0.061	146 ± 3	172	−14.9	−0.093	3562753
γ Oph	1340 ± 2	1320	19.1	0.014	729 ± 3	134	589	4.23	4931328
HR 6670	442 ± 0.5	456	−13.5	−0.030	78.2 ± 1.9	47.7	29.4	0.602	3563008
HR 7012	1410 ± 1	658	753	1.144	723 ± 5	73.3	649	8.85	3563264
η Tel	468 ± 0.7	333	135	0.405	469 ± 2	35.1	433	12.3	3563776
HD 181327	161 ± 0.3	154	7.1	0.046	555 ± 2	15.8	539	32.6	3564032
HD 191089	134 ± 0.4	131	3.0	0.023	363 ± 4	14.2	349	24.9	3564288
HD 200800	47.2 ± 0.3	43.0	4.2	0.097	9.5 ± 5.9	4.6	5.0	1.09	3582976
HR 8799	290 ± 0.4	280	10.5	0.038	72.1 ± 2.1	30.1	42.3	1.42	3565568
HD 221354‡	441 ± 0.5	469	−28.2	−0.060	43.4 ± 1.1	49.4	−7.1	−0.140	3565824

Note.—Double dagger (‡) signifies stars without strong IRS excess.

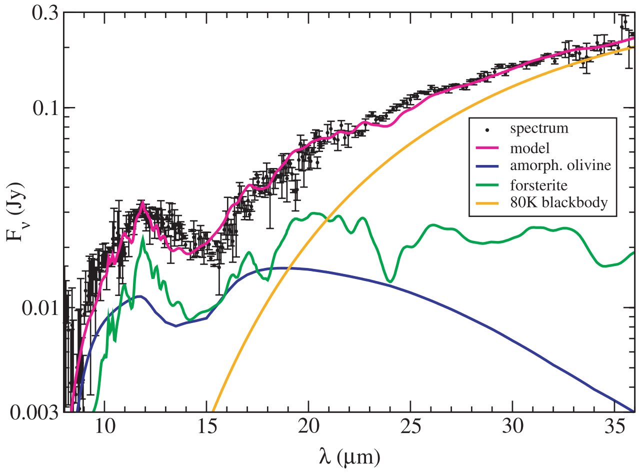

FIG. 2*a*

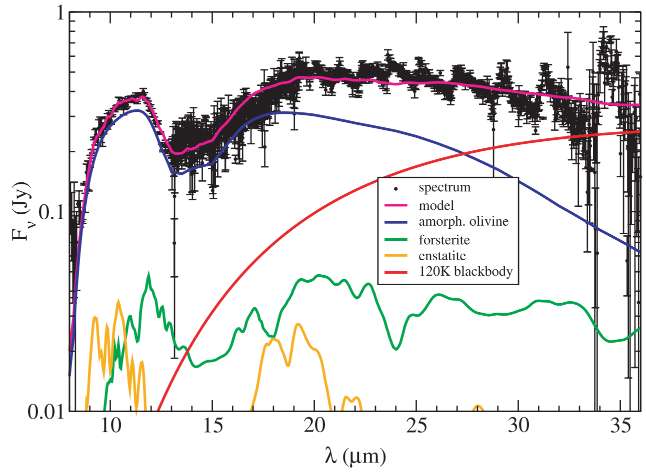

FIG. 2*b*

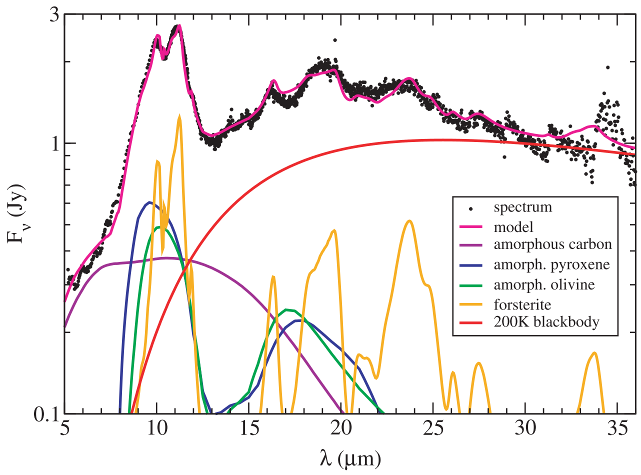

FIG. 2*c*

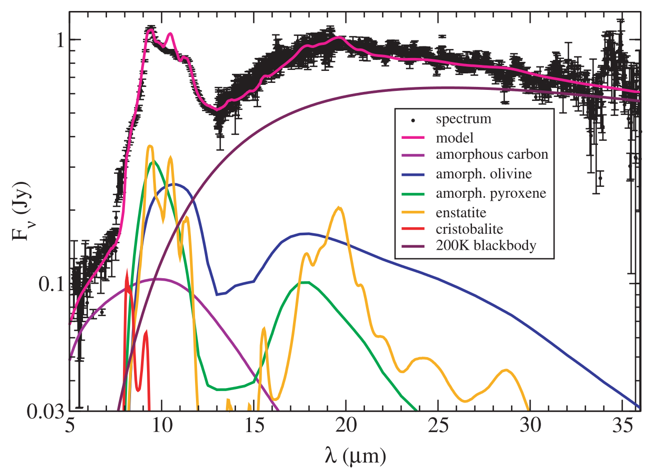

FIG. 2*d*

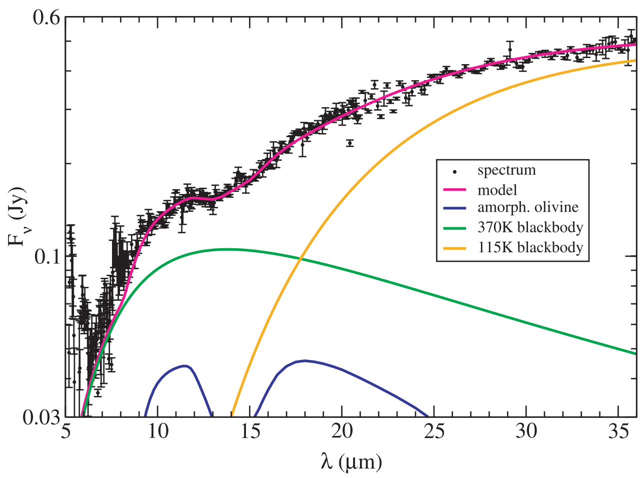

FIG. 2*e*

FIG. 2.—Photosphere-subtracted IRS spectra of (*a*) HR 3927, (*b*) η Crv, (*c*) HD 113766, (*d*) HR 7012, and (*e*) η Tel. The solid magenta lines show the final models for each disk system.

that the small particles in each system may have been generated in a recent collisions between parent bodies.

We are confident in the identification of silicate species around HD 113766, HR 7012, and η Crv; however, the exact dust mass in amorphous olivine, pyroxene, and carbon is somewhat uncertain. For example, for HD 113766, the presence of sharply peaked spectral features at 10.0, 11.1, 12.0, 16, 19, and 23.5 μm are used to identify forsterite. For HR 7012, the presence of spectral features at 9.3 and 10.5 μm are used to identify crystalline pyroxene. Once we fit the sharply peaked crystalline features, then we add amorphous olivine and pyroxene to fit the overall silicate feature; finally, we add amorphous carbon and one (or

TABLE 3
Spectral Feature Fitting Parameters

Parameter	HR 3927	η Crv	HD 113766	HR 7012	η Tel
Blackbody Components					
T_{bb1} (K)	80	120	200	200	115
Ω_{bb1} (10^{-16} sr)	350	80	68	42	160
T_{bb2} (K)	...	...	...	...	370
Ω_{bb1} (10^{-16} sr)	...	...	...	...	1.1
Temperatures					
$T_{silicate}$ (K)	290	360	600	520	370
T_{carbon} (K)	...	...	600	520	...
Silicate $a_{min,0}$ (μm)	3.1	0.54	1.4	1.1	2.4
Carbon $a_{min,0}$ (μm)	...	...	1.9	1.4	...
Silica $a_{min,0}$ (μm)	...	...	...	1.6	...
Amorphous Olivine Properties					
Composition	$MgFeSi0_4$	$MgFeSi0_4$	$MgFeSi0_4$	$MgFeSi0_4$	$MgFeSi0_4$
Shape	Spheres	Spheres	Spheres	Spheres	Spheres
a (μm)	3.1	3.5	1.5	5.0	3.0
f (V_{vac}/V_{tot})	0	0.35	0	0.6	0
m (10^{20} g)	24	7.8	82	4.4	8.0
Amorphous Pyroxene Properties					
Composition	...	...	$Mg_{0.5}Fe_{0.5}Si0_3$	$Mg_{0.8}Fe_{0.2}Si0_3$	...
Shape	...	...	Spheres	Spheres	...
a (μm)	...	...	1.5	1.1	...
f (V_{vac}/V_{tot})	...	...	0	0	...
m (10^{20} g)	...	...	97	2.4	...
Forsterite Properties					
Composition	$Mg_{1.9}Fe_{0.1}Si0_4$	$Mg_{1.9}Fe_{0.1}Si0_4$	Mg_2Si0_4	...	...
Shape	Spheres	Spheres	Nonspheres	...	...
a (μm)	8	8	Sub-μm	...	...
f (V_{vac}/V_{tot})	0	0	0	...	...
m (10^{20} g)	15	0.47	7.7	...	...
Enstatite Properties					
Composition	...	$MgSi0_3$	...	$Mg_{0.7}Fe_{0.3}Si0_4$	...
Shape	...	Spheres	...	Nonspheres	...
a (μm)	...	1	...	Sub-μm	...
f (V_{vac}/V_{tot})	...	0.4	...	0	...
m (10^{20} g)	...	3	...	20	...
Silica Properties					
Composition	...	...	...	Cristobalite	...
Shape	...	...	...	CDE2	...
a (μm)	...	...	...	Rayleigh limit	...
f (V_{vac}/V_{tot})	...	...	...	0	...
m (10^{20} g)	...	...	...	1.5	...
Amorphous Carbon Properties					
a (μm)	...	...	1.9	1.5	...
f (V_{vac}/V_{tot})	...	...	0	0	...
m (10^{20} g)	...	...	55	0.7	...

two) blackbodies to fit the remaining continuum. The fit to the noncrystalline component of the spectrum is degenerate and may be fitted with different ratios of amorphous silicates. In addition, the emissivity of amorphous carbon is approximately constant at 5–35 μm, suggesting that a blackbody could be substituted for this component. In the case of HR 7012, we use cristobalite because it produces a better fit to the 8.7 μm shoulder of the 10 μm silicate feature than alpha quartz; however, other silicates such as opal (hydrous silicate) may also provide good fits.

The majority of debris disks with spectral features possess crystalline silicate emission features; only η Tel in our sample does not. We estimate crystalline silicate mass fractions of 76%

and 0% for HR 7012 and η Tel (two $\sim$12 Myr old members of the β Pic moving group), 4.1% for HD 113766 (a $\sim$16 Myr old member of Sco-Cen), 38% for HR 3927 (a $\sim$50 Myr old field A-type main-sequence star), and 31% for η Crv (a $\sim$1 Gyr old field F-type main-sequence star). The crystalline silicate fraction for HR 7012 appears extremely high; however, those of the other debris disks are consistent with measurements toward pre–main-sequence T Tauri and Herbig AeBe stars (Sargent et al. 2006; Bouwman et al. 2001). Therefore, we find no correlation between age and crystallinity for circumstellar silicates. The most dramatic example of the lack of correlation between crystalline silicate fraction and age is the disparity in the crystallinity of the dust around HR 7012 and η Tel, both A-type main-sequence members of the β Pic moving group (Zuckerman et al. 2001).

Our solar system is believed to possess two populations of dust grains produced by collisions in two distinctive small body belts: (1) the zodiacal dust located at $D = 2$–4 AU with $T_{\rm gr} = 270$ K (Reach et al. 2003), generated by collisions between asteroids and (2) another population of cooler dust at $D = 30$–50 AU, with $T_{\rm gr} = 50$–60 K, that is believed to be generated by collisions between objects in the Kuiper Belt; this population of dust has not been detected directly thus far. Each of our systems with spectral features possesses at least two distinctive dust populations: a hot population with $T_{\rm gr} = 290$–600 K that is inferred to exist from detailed fitting of amorphous and crystalline silicate features, and a cooler population with $T_{\rm gr} = 80$–200 K that is inferred to exist from blackbody fits to the excess continuum. In addition, η Crv possesses a third, even colder dust component with $T_{\rm gr} = 40 \pm 5$ K, inferred from SED fits to *IRAS* 12–100 μm and JCMT SCUBA 450 and 850 μm photometry (Wyatt et al. 2005). Our results establish the presence of multiple belts of small bodies in debris disks; previously, the evidence was much weaker. The "hot" dust component in these systems is only 2.5–3.6 times hotter than the "cold" dust component, while zodiacal dust is estimated to be 4–5 times hotter than dust in the Kuiper Belt. HR 3927, η Crv, HD 113766, HR 7012, and η Tel may possess asteroid and Kuiper belts analogous to our solar system at larger distances from their central stars because of their higher luminosity. For η Crv, the detection of three planetesimal belts with blackbody distances of 1.3, 11, and 102 AU, respectively, may imply the presence of planets at 2.6, 22, and 204 AU (comparable to the distances of Mars, Saturn, and Sedna) if these belts are stirred by planets in the same way that the main asteroid belt is stirred by Jupiter in our solar system. Detailed dynamical models of this system are required to determine whether η Crv possesses multiple planets.

5. DUST PROPERTIES

The majority of infrared excess sources in our sample apparently lack spectral features, suggesting that the grains are too cold or too large ($a > 10$ μm) to produce features. We fit, using χ^2 minimization, the 5–35 μm photosphere-subtracted spectra for stars without silicate emission features, assuming that the grains are blackbodies. The photosphere-subtracted IRS spectra for all excess sources without spectral features are shown in Figure 3. The majority of our objects were observed in spectral mapping mode in which the slit is moved across the source, producing six independent spectra for each object. The error bars in this figure represent the difference between the two spectra in which the source is best centered. We overlaid our best-fit single-temperature blackbody model in blue. We list the best fitting grain temperatures, $T_{\rm gr}$, and fractional infrared luminosities, $L_{\rm IR}/L_*$, inferred for each system assuming $L_{\rm IR} = 4\Omega\sigma T_{\rm gr}^4 d^2$, where Ω is the solid angle subtended by the grains (in steradian) and d is the distance from the Sun to the central star, in Table 4 with the reduced χ^2 for each fit. Since no significant excess is detected toward τ Cet, despite a strong submillimeter excess characterized by $T_{\rm gr} = 60$ K, populations of cold dust may not be detected using IRS. Similarly, the temperatures inferred for cool dust populations using IRS spectra may be inaccurate.

The minimum grain distance can be constrained from the grain temperature, $T_{\rm gr}$, assuming that the dust particles act like blackbodies. Blackbodies in radiative equilibrium with a stellar source are located a distance

$$D = \frac{1}{2}\left(\frac{T_{\rm eff}}{T_{\rm gr}}\right)^2 R_* \quad (3)$$

from the central star (Jura et al. 1998), where $T_{\rm eff}$ and R_* are the effective temperature of the stellar photosphere and the stellar radius. We estimate the stellar temperatures and absolute V-band magnitudes from Strömgren photometry using the calibration of Napiwotzki et al. (1993) corrected for rotation (Figueras & Blasi 1998) and infer luminosities using the bolometric correction from Flower (1996). We estimate R_* assuming $L_* = 4\pi R_*^2 \sigma T_*^4$. The blackbody grain distances (listed in Table 4) range between 4 AU for the K1 V star HD 53143 and 72 AU for the B8 Vn star λ Cas.

We estimate the average grain size of orbiting dust grains assuming that radiation pressure removes grains with radii $<a_{\rm min,0}$ (please see eq. [1]) and that the dust grain size distribution is determined by collisional equilibrium (Greenberg & Nolan 1989):

$$n(a)\,da = n_0 a^{-p}\,da, \quad (4)$$

with $p \simeq 3.5$, similar to that inferred for the interstellar medium based on interstellar extinction curves, even though the grain-size distributions in these systems are not well constrained. Interplanetary and lunar size distributions with $p_{\rm small} = 2.2$–3.7 for grains with $a = 0.3$–2 μm and $p_{\rm large} = 2.0$ for grains with $a = 2$–20 μm have been used to reproduce *ISO* 5–16 μm observations of zodiacal dust (Reach et al. 2003). If we weight by the number of particles, we estimate average grain sizes, $\langle a \rangle = 5/3 a_{\rm min,0}$ (see Table 4), assuming that the density of an individual grain $\rho_s = 2.5$ g cm^{-3}. The majority of the stars in our sample are B-, A-, and F-type stars. (HD 53134 is the only object with infrared excess discussed here with spectral type later than F.) Since the radiation from these objects is dominated by optical and ultraviolet light, we expect that $2\pi a/\lambda \gg 1$, and therefore the effective cross section of the grains can be approximated by their geometric cross section so $Q_{\rm pr} \approx 1$. We estimate the stellar mass by fitting our inferred $T_{\rm eff}$ and log g to the Schaller et al. (1992) isochrones for B- and A-type stars and by fitting our inferred $T_{\rm eff}$ and L_* to Siess et al. (2000) isochrones for the remaining stars. We find average grain sizes between 0.2 μm for HD 53143 and 25 μm, for the B8 Vn star λ Cas (see Table 4), similar to those inferred for the zodiacal dust in our solar system (Reach et al. 2003).

We can estimate the minimum mass of dust around objects in our sample assuming that the particles have radius $a_{\rm min,0}$; if the grains are larger, then our estimate is a lower bound. If we assume a thin shell of dust at distance, D, from the star and if the particles are spheres of radius a and if the absorption cross section of the particles equals their geometric cross section, then the mass of dust is

$$M_{\rm dust} \geq \frac{16}{3}\pi \frac{L_{\rm IR}}{L_*} \rho_s D^2 a_{\rm min,0} \quad (5)$$

(Jura et al. 1995), where $L_{\rm IR}$ is the luminosity of the dust. We estimate dust masses in micron-sized infrared emitting grains between 3.7×10^{-8} $M_\oplus$ for HD 53143 and 2.3×10^{-4} $M_\oplus$ for the

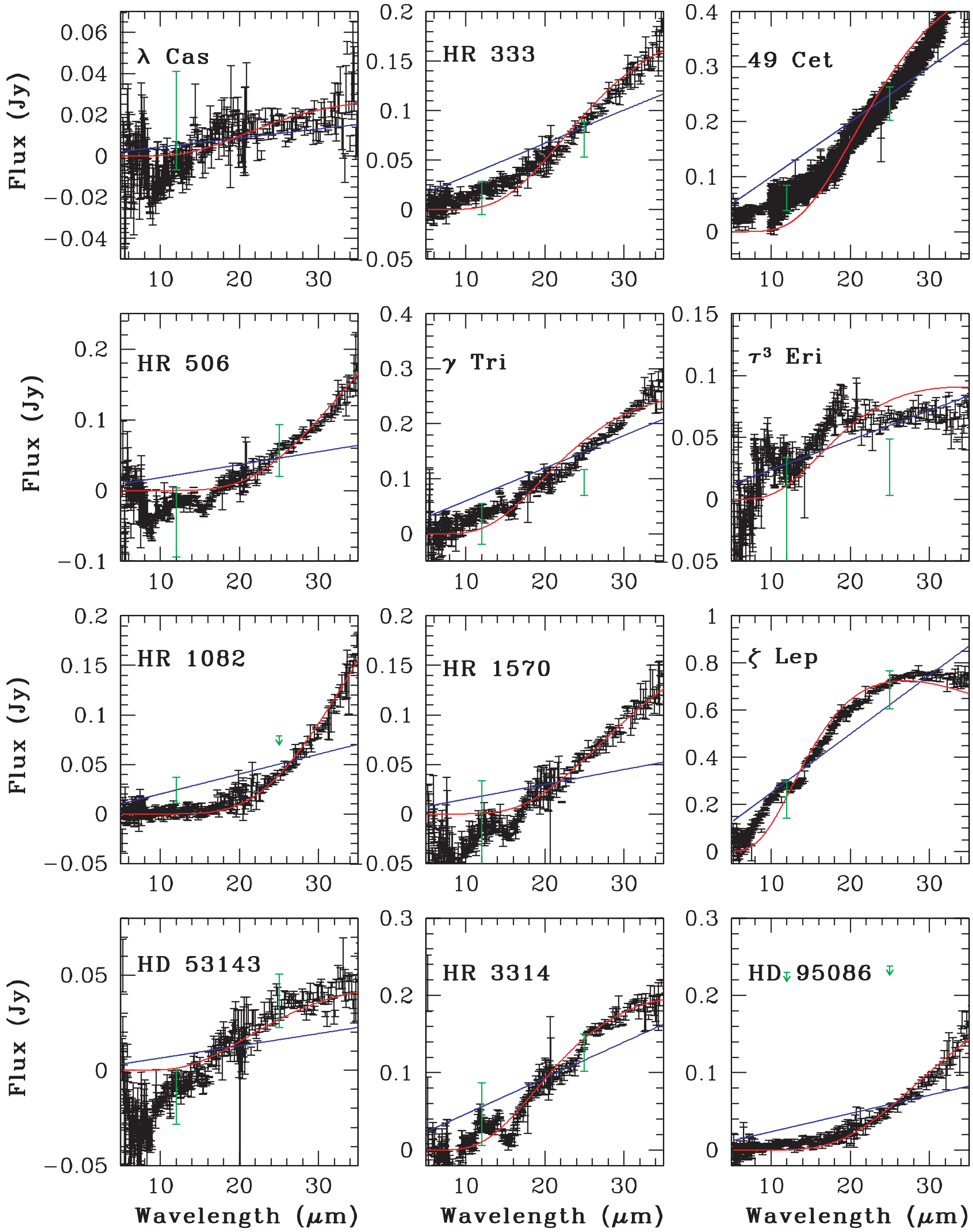

FIG. 3.—Photosphere-subtracted IRS spectra with F_ν plotted as a function of wavelength. The minimum χ^2 fits for the single-temperature blackbody and continuous disk models are overplotted in red and blue, respectively. *IRAS* photosphere-subtracted fluxes, where available, are overplotted in green to highlight any discrepancies with IRS data.

A3 IV/V star HR 1082 (see Table 4). If the grains possess a size distribution $n_0 a^{-3.5}$ with a maximum radius $a_{\rm max} = 10$ cm, as inferred from submillimeter observations (Zuckerman et al. 1995), we can estimate a the dust mass in larger grains. If the measured excess flux is F_ν(excess) and the blackbody flux for the excess is B_ν(excess), at frequency, ν, then

$$M_{10\,{\rm cm}} = \frac{4}{3}\rho\sqrt{a_{{\rm min},0}a_{\rm max}}\,d^2\,\frac{F_\nu({\rm excess})}{B_\nu({\rm excess})}, \tag{6}$$

where d is the distance to our Sun. We use the solid angle subtended by the dust grains, inferred from the minimum χ^2 blackbody fits to the excess, Ω, to determine the flux-to-blackbody ratio, $F_\nu({\rm excess})/B_\nu({\rm excess}) = \Omega$ and list the estimated larger grain dust masses in Table 4.

6. DUST REMOVAL MECHANISMS

Dust grains in debris disks may be removed by a variety of processes such as radiation and corpuscular stellar wind pressure, ice sublimation, and collisions. Collisions may shatter parent bodies into small grains that are radiatively drive grains from the system. Larger grains in these high-density environments may continue to collide until they reach sizes below the blowout limit and are radiatively ejected. In lower density disks around B- and

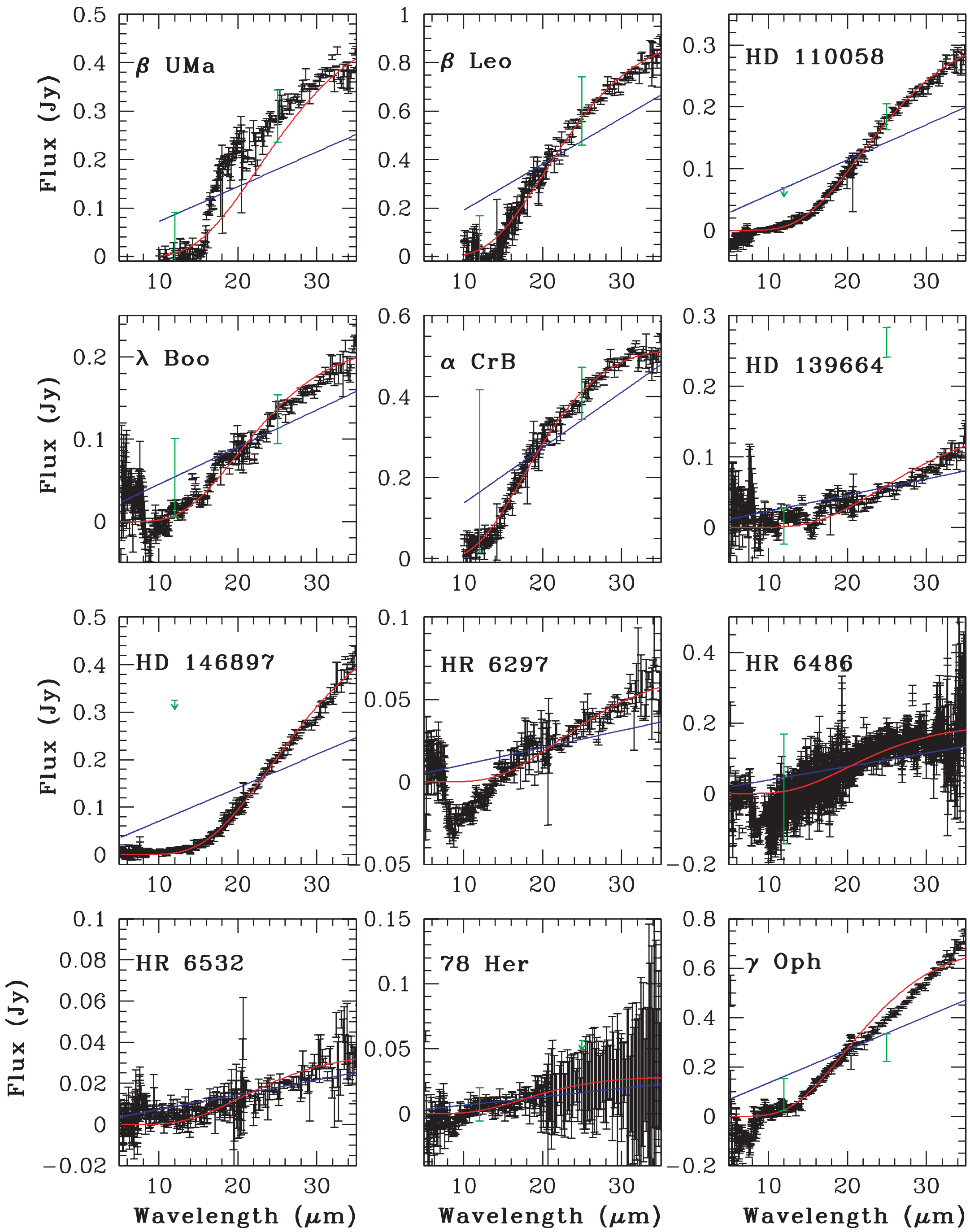

Fig. 3.—*Continued*

A-type main-sequence stars, large grains may be subject to the Poynting-Robertson effect and may spiral in toward the central star. In the absence of planets in our solar system, Poynting-Robertson and corpuscular solar wind drag would determine the spatial distribution of dust. The discovery of debris disks around lower mass solar-like and M-type stars has led to speculation that corpuscular stellar winds may contribute to grain removal in a manner analogous to radiation pressure and the Poynting-Robertson effect (Plavchan et al. 2005): (1) An outflowing corpuscular stellar wind produces a pressure on dust grains that overcomes the force due to gravity for small grains. (2) Particles orbiting the star are subject to a drag force produced when dust grains collide with atoms in the stellar wind. These collisions decrease the velocity of orbiting dust grains and therefore their angular momentum, causing them to spiral into the central star.

The dominant grain removal process within a disk is dependent not only on the luminosity of the central star but also on grain distance from the central star. For Fomalhaut, Backman & Paresce (1993) estimate that at 67 AU collisions to sizes below the blowout limit (grains below the blowout limit are quickly radiatively ejected from the system) are the most effective grain removal mechanism, while at 1000 AU the Poynting-Robertson effect is the most efficient grain removal process. In Figure 4, we plot the sublimation lifetime, the Poynting-Robertson (and corpuscular stellar wind) drag lifetime, and the collision lifetime for average-sized grains around typical B5 V, A5 V, and F5 V stars.

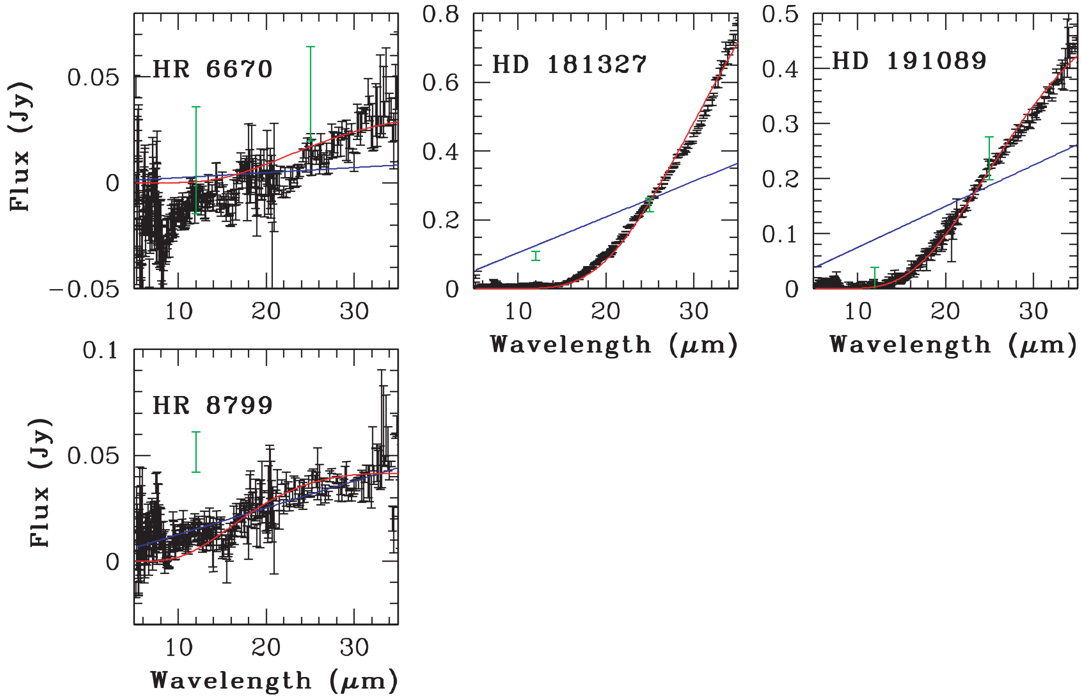

FIG. 3.—*Continued*

TABLE 4
DUST PROPERTIES INFERRED FROM EXCESS CONTINUA

Name	L_* ($L_\odot$)	M_* ($M_\odot$)	T_{gr} (K)	L_{IR}/L_*	D (AU)	$\langle a \rangle$ (μm)	M_{dust} ($M_\oplus$)	$M_{10\,cm}$ ($M_\oplus$)	Blackbody Minimum χ^2	K2 (Jy μm^{-1})	Uniform Disk Minimum χ^2
λ Cas	250	4.0	120 ± 100	4.4×10^{-6}	72	25	8.9×10^{-5}	0.007	4.4	4.4	5.4
HR 333	41	2.5	110 ± 15	9.8×10^{-5}	34	6.4	1.1×10^{-4}	0.02	7.8	33	31
49 Cet	19	2.2	118 ± 6	3.0×10^{-4}	22	3.5	7.7×10^{-5}	0.01	7.6	100	19
HR 506	1.7	1.2	70 ± 110	1.5×10^{-4}	21	0.6	5.1×10^{-6}	0.006	9.9	18	34
γ Tri	54	2.6	120 ± 15	2.2×10^{-5}	31	8.1	2.7×10^{-5}	0.003	8.4	56	24
τ^3 Eri	13	2.0	150 ± 20	2.1×10^{-5}	12	2.5	1.2×10^{-6}	0.0002	15	24	17
HR 1082	11	1.9	70 ± 70	4.2×10^{-4}	52	2.1	3.8×10^{-4}	0.07	2.9	20	48
HR 1570	22	2.2	90 ± 60	2.9×10^{-5}	42	3.9	3.2×10^{-5}	0.005	25	15	46
ζ Lep	30	2.3	191 ± 3	6.5×10^{-5}	10	5.0	5.6×10^{-6}	0.0008	36	250	83
HD 53143	0.48	0.8	120 ± 60	1.0×10^{-4}	4	0.2	6.1×10^{-8}	0.00003	2.4	6.4	23
HR 3314	43	2.5	130 ± 15	2.5×10^{-5}	27	6.8	1.9×10^{-5}	0.002	12	46.5	33
HD 95086	7.5	1.7	80 ± 30	6.4×10^{-4}	30	1.8	1.7×10^{-4}	0.03	5.1	23	46
β UMa	80	2.7	110 ± 30	1.1×10^{-5}	53	12	5.3×10^{-5}	0.005	30	72	72
β Leo	14	2.0	120 ± 15	2.7×10^{-5}	19	2.7	4.2×10^{-6}	0.0007	2.3	190	38
HD 110058	10	?	112 ± 7	1.0×10^{-3}	20	?	?	?	4.3	57	170
λ Boo	21	2.2	120 ± 20	3.2×10^{-5}	23	3.8	9.7×10^{-6}	0.001	11	45	23
α CrB	85	2.7	139 ± 7	1.3×10^{-5}	33	12	2.7×10^{-5}	0.002	3.5	140	54
HD 139664	3.6	2.7	100 ± 60	3.8×10^{-5}	15	1.0	1.2×10^{-6}	0.0003	7.0	23	7.5
HD 146897	4.6	1.5	100 ± 8	5.4×10^{-3}	17	1.2	2.9×10^{-4}	0.06	4.2	70	240
HR 6297	11	1.8	110 ± 40	5.1×10^{-5}	21	2.3	8.1×10^{-6}	0.001	8.4	10	15
HR 6486	6.8	1.7	120 ± 20	6.7×10^{-5}	14	1.6	3.3×10^{-6}	0.0006	4	38	6.9
HR 6532	93	3.0	120 ± 60	2.9×10^{-5}	47	12	1.2×10^{-4}	0.01	3.1	7.2	3.6
78 Her	51	2.6	140 ± 160	1.6×10^{-5}	23	19	2.5×10^{-5}	0.002	0.5	6.5	0.7
γ Oph	39	2.5	124 ± 9	5.2×10^{-5}	27	6.1	3.8×10^{-5}	0.005	29	130	120
HR 6670	4.1	1.5	110 ± 120	2.4×10^{-5}	13	1.1	7.4×10^{-7}	0.0002	7.3	2.4	9.6
HD 181327	2.5	1.9	81 ± 7	3.1×10^{-3}	20	0.9	1.7×10^{-4}	0.04	21	104	1500
HD 191089	3.1	1.8	99 ± 9	1.5×10^{-3}	14	0.9	4.4×10^{-5}	0.01	3.6	75	220
HR 8799	6.1	1.6	150 ± 30	4.9×10^{-5}	8	1.5	7.2×10^{-7}	0.0002	4.7	13	3.1

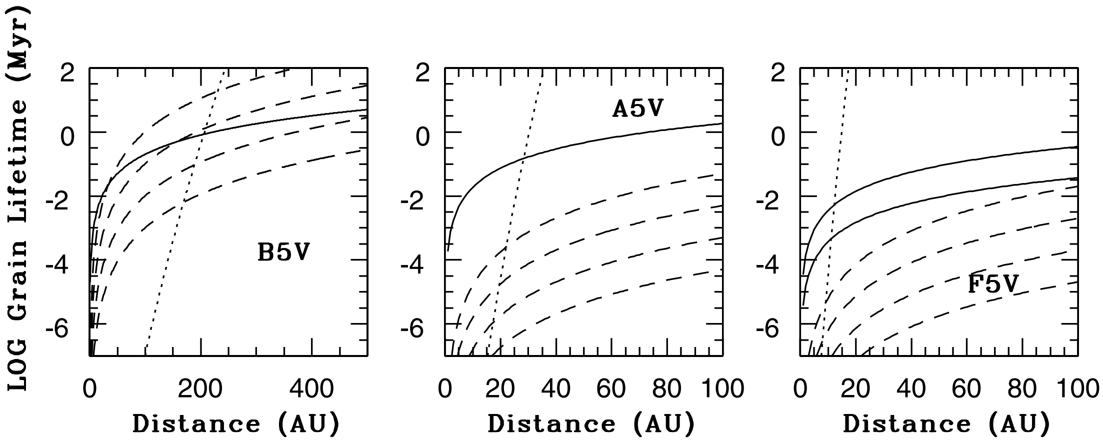

FIG. 4.—(*a*) Grain lifetimes are plotted as a function of distance around a B5 V star. The Poynting-Robertson Drag/Stellar Wind drag lifetime is shown with a solid line; the sublimation lifetime is showed with a dotted line; and the collisional lifetime is shown with a dashed line, assuming $M_{\rm submm} = 0.001, 0.01, 0.1$, and 1 $M_\oplus$ (*from top to bottom*). (*b*) Same as (*a*) for A5 V star. No stellar wind drag is assumed. (*c*) Same as (*a*) for a F5 V star. The Stellar Wind drag lifetime is shown with a solid line, assuming that $\dot{M}_{\rm wind} = 100, 1000\ \dot{M}_\odot$ (*from top to bottom*).

Sublimation may quickly remove icy grains in the innermost portions of the disk. At larger radii, collisions dominate grain destruction, and at the largest radii, where the disk has the lowest density, Poynting-Robertson and corpuscular stellar wind drag may dominate grain destruction. We estimate the lifetimes of average-sized grains and the parent body masses around stars in our sample if ice sublimation, Poynting-Roberton and corpuscular stellar wind drag, and collisions are each the dominant grain removal mechanism in the absence of other processes.

6.1. *Ice Sublimation*

One possible explanation for the presence of central clearings, inferred from blackbody fits to the IRS spectra, is that the grains are icy and sublimate when they come too close to the central star. Although the dust grain composition cannot be determined directly from spectral features, it may be inferred from the statistical grain properties in our sample. We plot the distribution of inferred grain temperatures in Figure 5. The estimated grain temperatures appear to cluster between 110 and 130 K. Laboratory studies find that thermal desorption of water ice (H_2O) from H_2O layers begins at temperatures of 120 K and is completed by 170 K (Fraser et al. 2001). Therefore, the peak in grain temperature at 110–120 K may suggest that the grains are icy and are beginning to sublimate.

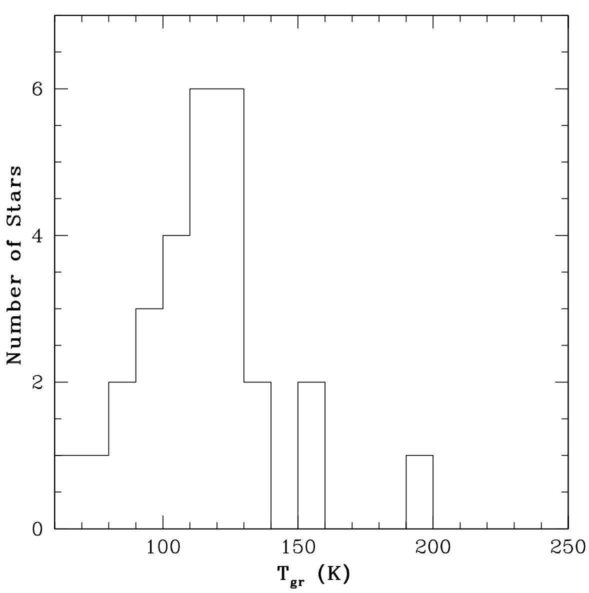

FIG. 5.—Histogram showing the distribution of inferred blackbody grain temperatures for objects whose IRS spectra are well fitted by a single-temperature blackbody.

If the grains are icy, then sublimation may also remove grains from the disk. If the grain temperature is constant while the star remains on the main sequence, then we may write the following expression for the sublimation lifetime of an average grain:

$$t_{\rm subl} = \frac{\langle a \rangle \rho_i T_{\rm gr}^{1/2} e^{T_{\rm subl}/T_{\rm gr}}}{\dot{\sigma}_0} \tag{7}$$

(Jura et al. 1998), where $\dot{\sigma}_0$ is the mass rate per surface area ($=3.8 \times 10^8$ g cm^{-2} s^{-1} K$^{1/2}$, $T_{\rm subl} = 5530$ K; Ford & Neufeld 2001) and $\rho_i = 1.5$ g cm^{-3} if the grains are mostly ice with some refractory material mixed in, as expected for Kuiper Belt objects. The average grain radius, $\langle a \rangle$, listed in Table 4 is computed assuming that the grains are composed of silicates with $\rho_s = 2.5$ g cm^{-3}; therefore, if the grains are mainly composed of ices, then the estimated average grain radii are an underestimate and the values in this table should be multiplied by 5/3. We list the sublimation lifetimes for grains in Table 5 assuming that they are icy. The sublimation lifetimes are sensitively dependent on grain temperature. For example, 3.5 μm grains around HR 1082 with an estimated $T_{\rm gr} = 70$ K, have a sublimation lifetime, $T_{\rm subl} = 1.3 \times 10^7$ Gyr, while 16 μm grains around HR 6211 with an estimated $T_{\rm gr} = 160$ K have a sublimation lifetime, $T_{\rm subl} = 7.4$ minutes. In systems with $T_{\rm gr} > 100$ K, the sublimation lifetime is the shortest lifetime by more than an order of magnitude.

6.2. *Poynting-Robertson Drag*

If Poynting-Robertson (PR) drag is the dominant grain removal mechanism, then grains spiral in from the radii at which they are created toward their orbit center, creating a continuous disk with uniform surface density and a $1/D$ volume density. In this model, the inner radius of the disk coincides with the stellar radius unless the grains sublimate or are dynamically ejected by a massive body interior to the radius at which the grains are produced. For an optically thin, gas-free disk whose particle density, n, varies

TABLE 5
Dust Removal Mechanisms

Name	$(\dot{M}_{\rm wind}c^2)/L_*$	PR Drag $t_{\rm PR}$ (Myr)	PR Drag $M_{\rm PB}$ ($M_\oplus$)	CPR Drag $t_{\rm PR+wind}$ (Myr)	CPR Drag $M_{\rm PB}$ ($M_\oplus$)	Collision $t_{\rm coll}$ (Myr)	Sublimation $t_{\rm subl}$ (Myr)
λ Cas	1.4	0.88	0.012	0.36	0.0034	1.9	7.3×10^{-4}
HR 333	...	0.31	0.040	...	...	0.034	7.8×10^{-3}
HR 506	82	0.24	0.0063	0.003	0.13	0.020	1.1×10^{8}
49 Cet	...	0.15	0.058	...	...	0.0073	9.3×10^{-5}
γ Tri	...	0.25	0.019	...	...	0.14	3.0×10^{-5}
τ^3 Eri	...	0.049	0.012	...	...	0.057	3.1×10^{-9}
HR 1082	...	0.93	0.061	...	...	0.025	1.3×10^{10}
HR 1570	...	0.54	0.013	...	...	0.22	2.0×10^{2}
ζ Lep	...	0.031	0.032	...	...	0.011	3.5×10^{-12}
HD 53143	?	0.014	0.0013	?	?	0.0036	1.5×10^{-5}
HR 3314	...	0.20	0.018	...	...	0.11	3.9×10^{-6}
HD 95086	...	0.37	0.0071	...	...	0.0081	7.3×10^{3}
β UMa	...	0.69	0.026	...	...	0.7	2.7×10^{-2}
β Leo	...	0.12	0.0049	...	...	0.080	3.8×10^{-5}
HD 110058	...	...	0.015	...	...	...	...
λ Boo	...	0.16	0.017	...	...	0.085	2.5×10^{-5}
α CrB	...	0.26	0.031	...	...	0.28	3.4×10^{-7}
HD 139664	?	0.10	0.0059	?	?	0.058	1.7×10^{-1}
HD 146897	?	0.13	0.011	?	?	0.00042	1.4×10^{-1}
HR 6297	...	0.17	0.021	...	...	0.027	2.0×10^{-3}
HR 6486	...	0.08	0.0099	...	...	0.026	1.2×10^{-5}
HR 6532	1.2	0.48	0.050	0.17	0.015	0.2	2.2×10^{-4}
78 Her	...	0.34	0.0036	...	...	0.29	4.3×10^{-7}
γ Oph	...	0.20	0.034	...	...	0.052	2.3×10^{-5}
HR 6670	190	0.081	0.015	0.00043	0.69	0.068	1.9×10^{-3}
HD 181327	?	0.24	0.99	?	?	0.0013	6.0×10^{4}
HD 191089	?	0.11	0.65	?	?	0.0014	2.7×10^{-1}
HR 8799	...	0.027	0.016	...	...	0.014	1.3×10^{-9}

as D^{-q}, the infrared spectrum should be well described by the function

$$F_\nu = K_1 B_\nu(T_*) + K_2 \nu^{-3+2q+0.5pq-0.5p} \quad (8)$$

(Jura et al. 1998), where the absorption coefficient for the grains $Q_{\rm abs} \propto \nu^p$ and K_1 and K_2 are constants. The first term describes the photospheric emission and the second the infrared excess. If the grains are large ($p = 0$) and the surface density is determined by PR drag ($q = 1$), then the infrared spectrum, $F_\nu \propto \nu^{-1}$. We plot the minimum χ^2 fits to the IRS photosphere-subtracted spectra in blue in Figure 3, assuming that the grains are large ($p = 0$) and list the fitting parameter K_2 in Table 4 along with the minimum reduced χ^2 for the fits. The continuous disk model has a lower reduced χ^2 than the single-temperature blackbody for one object in our sample (HR 8799); however, this source possess a weak IRS excesses (<0.1 Jy) that is detected with SNR < 5.

Our simple SED models suggest that PR drag may not be the dominant grain removal mechanism in debris disks. To test this hypothesis, we compare the PR drag lifetimes and the lifetimes for grains under sublimation, corpuscular stellar wind drag, and collisions for all of the sources in our study. The PR drag lifetime of grains in a circular orbit, a distance D from a star is

$$t_{\rm PR} = \left(\frac{4\pi\langle a\rangle\rho_s}{3}\right)\frac{c^2 D^2}{L_*} \quad (9)$$

(Burns et al. 1979). The PR drag lifetimes of average-sized grains (12,000 yr–1.1 Myr; see Table 5), estimated using the grain properties in Table 4, are significantly shorter than the stellar ages ($t_{\rm age}$), suggesting that the grains are replenished through collisions between larger bodies. The PR drag lifetime of average-sized grains around HR 8799, the only object whose excess spectrum is better modeled by $F_\nu \propto \lambda$, is not the shortest grain lifetime by a factor of 2; therefore, we do not expect that this system should possess a uniform disk. We estimate lower limits for the parent body masses around our objects assuming that all of the grains are destroyed by PR drag and that the systems are in steady state. If $M_{\rm PB}$ denotes the mass in parent bodies, then we may write

$$M_{\rm PB} \geq \frac{4 L_{\rm IR} t_{\rm age}}{c^2} \quad (10)$$

(Chen & Jura 2001). We estimate the infrared luminosities of the systems from the blackbody fits to the excess. If the grains emit a substantial fraction of their radiation at $\lambda > 30$ μm, then this approximation may not be valid. The inferred parent body masses range between 1.3×10^{-3} $M_\oplus$ for the K1 V star HD 53143 and 0.93 $M_\oplus$ for the A3 IV/V star HR 1082 (see Table 5).

Whether PR drag or other processes, such as collisions, are the dominant grain destruction mechanism in debris disks is uncertain and depends on the density of dust grains and the spatial distribution of dust for each particular object. Numerical models of the dynamical evolution of dust in collisional equilibrium suggest that Poynting-Robertson drag is the primary mechanism for grain transport in disks with $L_{\rm IR}/L_* \leq 10^{-6}$, while radiation pressure is the primary mechanism for dust transport in collisionally dominated disks with $L_{\rm IR}/L_* \geq 10^{-4}$ (Krivov et al. 2000).

Recently, Wyatt (2005) concluded that PR drag is relatively unimportant in *IRAS*-discovered debris disks. He found that the volume density of grains in *IRAS*-discovered debris disks is so high that grains that migrate inward under Poynting-Robertson drag will suffer destructive collisions with other grains and will be rapidly expelled by radiation pressure. The destruction of inward-migrating dust grains via mutual collisions may explain the presence of central clearings without requiring the presence of icy grains or planets in debris disks.

6.3. *Stellar Wind Drag*

For B-type main-sequence stars and young solar-like main-sequence stars, both of which possess strong stellar winds, drag on dust grains produced by loss of angular momentum to corpuscular stellar wind may be stronger than that produced by the Poynting-Robertson effect. Stellar wind drag may explain the observed anticorrelation between *Spitzer* 24 μm excess and *ROSAT* fluxes toward F-type stars in the 3–20 Myr Sco-Cen (Chen et al. 2005) and the lack of 12 μm excesses observed toward nearby, >10 Myr old, late-type M dwarfs (Plavchan et al. 2005). Recently, Strubbe & Chiang (2006) have reproduced the radial brightness profile of the AU Mic disk assuming that collisions between parent bodies on circular orbits at 43 AU produce the observed dust grains. Large grains produce a surface density, $\sigma \propto r^0$, at $r <$ 43 AU, under corpuscular and Poynting-Robertson (CPR) drag modified by collisions, while small grains that are barely bound under corpuscular stellar wind and radiation pressure produce a surface density, $\sigma \propto r^{-5/2}$, in the outer disk.

Stellar winds around B-type stars are produced by the transfer of momentum from photons below the photosphere to material outflowing in the wind. The mass-loss rates and expansion velocities can be measured from radio observations of free-free emission produced in the outer parts of the wind or from Hα emission that may be formed in the inner regions of the wind. Monte Carlo simulations of stellar winds that include multiple scattering of photons successfully reproduce stellar wind mass-loss rates measured at radio wavelengths (Vink et al. 2000). We estimate the stellar mass-loss rates ($\dot{M}_{\rm wind}$) for the B-type stars in our sample using a fit to the numerical models of Vink et al. (2000) that depend on the stellar luminosity, mass, and effective temperature, assuming that the ratio of the terminal wind velocity to the effective wind escape velocity at the stellar surface, $v_\infty/v_{\rm esc} = 1.3$. The increase in "drag" in the inward drift velocity of dust grains under corpuscular stellar wind and Poynting-Robertson drag over that produced by Poynting-Robertson drag alone is given approximately by the factor $1 + \dot{M}_{\rm wind}c^2/L_*$ (Jura 2004).

The mass-loss rates due to stellar winds around 14 nearby, solar-like stars have been inferred via Lyα absorption, produced when the stellar wind collides with the surrounding interstellar medium, producing a hot H I astrosphere with an effective temperature 20,000–40,000 K (Wood et al. 2002, 2005). Wood et al. (2002, 2005) fitted the stellar mass-loss rate, $\dot{M}_{\rm wind}$, per stellar surface area, A, as a power-law function of X-ray flux per stellar area, $\dot{M}_{\rm wind}/A \propto F_{\rm X}^{1.34\pm0.18}$, assuming that the wind speed for solar-like stars is similar to that measured for the Sun, $v_{\rm wind} =$ 400 km s^{-1}. The uncertainty in the $\dot{M}_{\rm wind}$ extrapolation is probably a factor of 2 because the size of the astrosphere and the amount of astrospheric absorption scales as the square root of the wind ram pressure; the wind ram pressure $P_{\rm wind} \propto \dot{M}_{\rm wind}v_{\rm wind}$; and the variation in the solar wind speed is approximately a factor of 2. The stellar mass-loss rate power-law dependence on X-ray flux per stellar area saturates at $F_{\rm X} = 8 \times 10^5$ ergs cm^{-2} s^{-1}. One possible explanation for the saturation is that stars possess more polar spots as they become more magnetically active, indicating changes in the field geometry. Changes in the field structure could precipitate changes in the stellar wind (Wood et al. 2005).

We infer $\dot{M}_{\rm wind}$ from *ROSAT* fluxes for our sample assuming the Wood et al. (2005) power law, scaling to observations of α Cen ($F_{\rm X} = 3.7 \times 10^4$ ergs cm^{-2} s^{-1}, $\dot{M}_{\rm wind}/A = 0.9\,\dot{M}_\odot/A_\odot$); the astrosphere for this source is well-detected in Lyα and its $\dot{M}_{\rm wind}/A$ and $F_{\rm X}$ values lie on the published fit. We list the observed *ROSAT* fluxes, HR 1 hardness ratios between the 0.1–0.4 and the 0.5–2.0 keV bands, and the angular offsets between the *ROSAT* catalog sources and the FGKM-type stars in our sample in Table 6. The X-ray spectra for stars in our sample have flat spectral energy distributions, with a mean hardness ratio −0.4, consistent with observations of stars in the solar neighborhood. We estimate X-ray luminosities, $L_{\rm X}$, using the conversion 1 *ROSAT* count = (8.31 + 5.30 HR1) $\times 10^{-12}$ ergs cm^{-2} (Fleming et al. 1995). The inferred $F_{\rm X} > 8 \times 10^5$ ergs cm^{-2} s^{-1} for 8 solar-like and low-mass stars, suggesting that the stellar winds for these stars are probably 1 or 2 orders of magnitude smaller than inferred from the Wood et al. (2005) relation: τ^1 Eri, α For, HD 53143, HD 113766, HD 139664, HD 146897, HD 181327, and HD 191089. We do not make any extrapolations for the mass-loss rates in these systems.

For the B-type stars and solar-like and low-mass stars with $F_{\rm X} < 8 \times 10^5$ ergs cm^{-2} s^{-1}, $\dot{M}_{\rm wind}c^2/L_* > 1$, suggesting that stellar wind drag cannot be neglected (see Table 5). The lifetime for grains in a circular orbit under the Poynting-Robertson effect and stellar wind drag is

$$t_{\rm PR+wind} = \left(\frac{\dot{M}_{\rm wind}c^2}{L_*} + 1\right)^{-1} t_{\rm PR}. \tag{11}$$

We estimate the combined Poynting-Robertson and stellar wind drag lifetimes using the Poynting-Robertson drag time lifetimes and $\dot{M}_{\rm wind}c^2/L_*$ values listed in Table 5. For B-type stars, $\dot{M}_{\rm wind}c^2/L_*$ is typically $\sim$2; therefore, the drag lifetimes of the grains are reduced in most cases by $\sim$60%. For example, λ Cas and HR 6532 possess $\dot{M}_{\rm wind}c^2/L_* = 1.4$ and 1.2, respectively. However, for F-type and later stars, $\dot{M}_{\rm wind}c^2/L_*$ is typically $\sim$100 if the source is detected by *ROSAT*; therefore, the drag lifetimes of the grains are reduced by a factor of a couple hundred. For example, HR 506 and HR 6670 may possess $\dot{M}_{\rm wind}c^2/L_*$ as high as 82 and 190. Unfortunately, *ROSAT* upper limits do not place stringent upper limits on $\dot{M}_{\rm wind}c^2/L_*$ in cases in which the source is not detected. The mass in parent bodies assuming that the system is in steady state and that Poynting-Robertson drag and stellar wind drag are the dominant grain removal mechanisms is given by the expression

$$M_{\rm PB} \geq \left(\frac{\dot{M}_{\rm wind}c^2}{L_*} + 1\right)\frac{L_{\rm IR}}{c^2}\, t_{\rm age}. \tag{12}$$

We estimate the mass in parent bodies using the inferred stellar properties listed in Table 4. For B-type stars, the stellar wind drag inferred parent body masses are consistent with the PR drag inferred parent body masses, $M_{\rm PB} < 1\ M_\oplus$. However, for solar-like stars, the stellar wind drag inferred parent body masses are substantially (20–50 times) higher but still less than 1 $M_\oplus$. The fact that so little material remains in parent bodies suggests that planet formation must be an efficient process if planets have already formed in these systems.

6.4. *Collisions*

If the particle density within the disk is high, then collisions are expected to dominate grain destruction by generating small

TABLE 6
X-Ray and Stellar Wind Properties of FGKM Stars

Name	Offset (arcsec)	*ROSAT* (counts s^{-1})	HR1	F_X (ergs s^{-1} cm^{-2})	$\dot{M}_{wind}$ ($\dot{M}_\odot$)
107 PSC	0.13	0.027 ± 0.003	−0.92 ± 0.04	5.1×10^3	3.0
HR 506	0.46	0.092	−0.63 ± 0.03	1.7×10^5	290
HD 16157	0.10	3.52 ± 0.02	0.11 ± 0.01		
τ^1 Eri	0.04	0.72 ± 0.02	−0.25 ± 0.03	1.0×10^6	?
α For	0.20	2.8 ± 0.2	−0.08 ± 0.05	2.3×10^6	?
γ Dor	0.11	0.19 ± 0.04	−0.09 ± 0.18	6.7×10^5	2100
HR 1686	0.18	0.020 ± 0.007	−1.0 ± 0.4	1.5×10^4	26
HR 2483	...	<0.05	...	$<1.5 \times 10^5$	<260
HD 53143	0.48	0.19 ± 0.01	−0.37 ± 0.05	8.8×10^5	?
HR 3220	0.14	0.35 ± 0.03	−0.18 ± 0.09	7.1×10^5	4100
FI Vir	0.05	0.053	−0.50 ± 0.06		
HR 3862	0.07	0.002 ± 0.0007	...	$<2.9 \times 10^3$	<2.1
η Crv	0.02	0.21 ± 0.03	−0.48 ± 0.13	3.4×10^5	1100
HD 113766	...	<0.05	...	$<7.6 \times 10^6$	?
HR 5236	...	<0.05	...	$<7.2 \times 10^5$	<2200
σ Boo	0.11	0.17 ± 0.02	−0.32 ± 0.11	2.5×10^5	650
HD 139664	0.11	0.52 ± 0.04	−0.28 ± 0.06	1.2×10^6	?
HR 5933	0.35	0.04 ± 0.02	−0.90 ± 0.14	1.2×10^4	14
HD 146897	...	<0.05	...	$<5.6 \times 10^6$	?
HR 6670	0.03	0.10 ± 0.02	−0.50 ± 0.17	4.4×10^5	1700
HD 181327	...	<0.05	...	$<1.3 \times 10^6$	?
HD 191089	0.06	0.02 ± 0.02	−0.30 ± 0.22	1.4×10^6	?
HD 221354	...	<0.05	...	$<3.7 \times 10^4$	<160

grains that are removed rapidly via radiation and corpuscular stellar wind pressure. We estimate the collision lifetime assuming that grains are on inclined orbits, such that they encounter the surface density of the disk twice per orbit, that tangential collisions are destructive, and that they have a collisional equilibrium size distribution (given in eq. [4])

$$t_{coll} = 3000\ \mathrm{yr}(D/30\ \mathrm{AU})^{7/2}(M_{submm}/0.1\ M_\oplus)^{-1} \times(\sqrt{a_{min}a_{max}}/1\ \mathrm{mm})(M_\odot/M_*)^{1/2} \quad (13)$$

Backman & Paresce (1993) using grain distances, dust masses (extrapolated for micron-sized through centimeter-sized grains), and minimum radii in Table 4. For the majority of our systems, the collision lifetimes computed are comparable to or shorter than the Poynting-Robertson and/or stellar wind drag lifetimes (see Table 5), suggesting that collisions dominate the destruction of particles, consistent with published studies (Wyatt 2005; Dominik & Decin 2003; Najita & Williams 2005). In Figure 4, we plot the sublimation lifetime if the grains are icy, the Poynting-Robertson and stellar wind drag lifetime, and the collision lifetime as a function of radius around typical B5 V, A5 V, and F5 V stars. In all cases, sublimation is the dominant grain removal process at small distances from the star. For typical A5 V and F5 V stars, the collision lifetime for average-sized grains is shorter than the drag lifetime if the disk has a dust mass between 0.001 $M_\oplus$ and 1 $M_\oplus$, even if the F5 V star has a stellar wind with a mass-loss rate as high as $\dot{M}_{wind}$ = 1000 $\dot{M}_\odot$. However, for a typical B5 V star, the Poynting-Robertson and stellar wind drag lifetime may be shorter than the collision lifetime, especially at large radii, if the disk has a dust mass $M_{submm} \sim 0.1\ M_\oplus$; however, we infer small $M_{submm} = 1.0 \times 10^{-5}\ M_\oplus$ for some stars in our sample, suggesting that Poynting-Robertson and corpuscular stellar wind drag effects should be the dominant grain removal mechanism for at least some objects.

The fractional infrared luminosity of a debris disk for a fixed distance is expected to decrease inversely with time, $L_{IR}/L_* \propto 1/t_{age}$, if collisions are the dominant grain removal process and is expected to decrease inversely with time squared, $L_{IR}/L_* \propto 1/t_{age}^2$, if Poynting-Robertson drag is the dominant grain removal process (Dominik & Decin 2003). We plot L_{IR}/L_* as a function of age for the systems in our sample in Figure 6*a*. For young stars that do not appear on the Schaller et al. (1992) isochrones, we assume moving group ages rather than our assigned ages. The upper envelope of the distribution can be fitted with the function $L_{IR}/L_* = (L_{IR}/L_*)_0(t_0/t_{age})$, where $(L_{IR}/L_*)_0 t_0 = 0.40$ Myr; however, the function $L_{IR}/L_* = (L_{IR}/L_*)_0(t_0/t_{age})^2$, with $(L_{IR}/L_*)_0 t_0^2 = 60\ \mathrm{Myr}^2$ does not produce a bad fit. The $1/t^2$ trend line includes all of the sources in our sample except η Crv, which has a high $L_{IR}/L_* = 3 \times 10^{-4}$ for its age of 1 Gyr. Our data set is consistent with the idea that debris disks are collisionally dominated systems, but our data set is too small to determine whether Poynting-Robertson drag dominates grain removal at any particular age. A $1/t_{age}$ time dependence with a decay timescale $t_0 = 150$ Myr has been observed for the MIPS 24 μm and *IRAS* 25 μm excess around ~270 A-type stars, consistent with grain destruction via collisions (Rieke et al. 2005). Similarly, A $1/t_{age}$ time dependence with a decay timescale $t_0 = 200$ Myr has been observed for the 850 μm excess around 13 nearby, solar-like stars also consistent with grain destruction via collisions (Najita & Williams 2005). Our study differs from these in the Rieke et al. (2005) and the Najita & Williams (2005) samples in that (1) our sample contains a heterogenous mix of stars with varying spectral type and (2) our data set includes the measurement of the excess at more than one wavelength; the measurement of the SED allows us to infer the dust temperature and therefore the infrared luminosities and dust masses/dust production rates more accurately.

In a minimum mass solar nebula, 1000–3000 km-sized bodies are expected to grow on timescales, $t_P \approx 15-20\ \mathrm{Myr}\ (D/30\ \mathrm{AU})^3$ (Kenyon & Bromley 2004, 2005) and to perturb planetesimals in the disk, initiating collisional cascades that produce micron-sized grains. This model predicts a $t^{-0.6}$ to $t^{-0.35}$ decay of the fractional infrared luminosity for the whole debris disk at ages

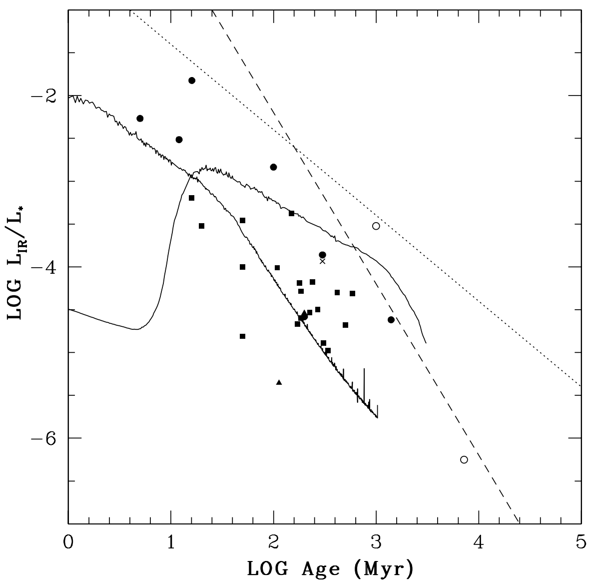

FIG. 6a

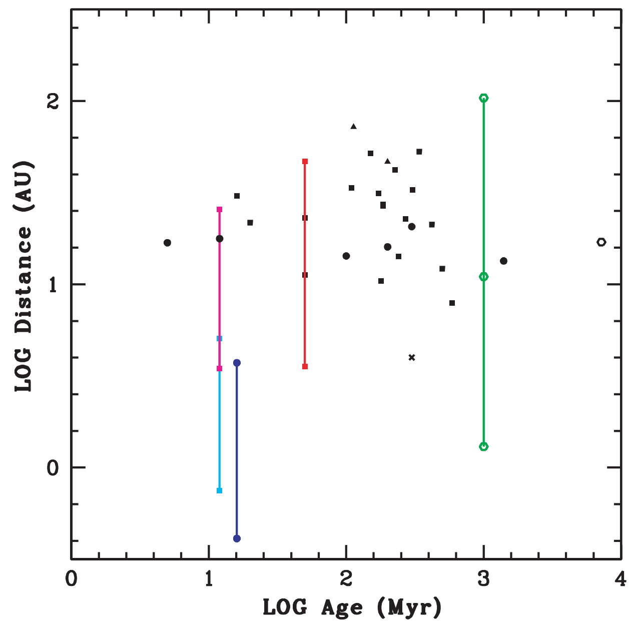

FIG. 6b

FIG. 6.—(*a*) Inferred fractional luminosity, L_{IR}/L_* plotted as a function of age. The solid lines show the Kenyon & Bromley (2005) model for the evolution of L_{IR}/L_* for dust at 3–20 AU (*left*) and at 30–100 AU (*right*) around a main-sequence A-type star. The dotted line shows the slope expected if the dust mass declines inversely with age as expected if collisions are the dominant grain destruction mechanism; HD 113766 and η Crv possess extremely high values of L_{IR}/L_* for their ages and define the fitting coefficient for the $1/t$ trend line. The dashed line shows the slope expected if Poynting-Robertson and corpuscular stellar wind drag are the dominant grain destruction mechanism; this trend line accounts for all of the stars in our sample except for η Crv. (*b*) Blackbody grain distance plotted as a function of stellar age. Stars with proposed multiple debris belts are shown in color with a line connecting multiple points. HR 3927, η Crv, HD 113766, HR 7012, and η Tel are shown in red, green, blue, cyan, and magenta, respectively. In both plots, B-type stars are shown with filled triangles; A-type stars are shown with filled squares; F-type stars are shown with filled circles; the K-type star is shown with a cross. The addition of submillimeter data to infer L_{IR}/L_* and D for η Crv and τ Cet (*open circles*) does not appear to elucidate either the relation between fractional infrared luminosity and age or grain distance and age.

of 10 Myr to 1 Gyr, depending on the tensile strength of the grains, a somewhat more shallow evolution of the fractional infrared luminosity than inferred by Dominik & Decin (2003). The Kenyon & Bromley (2004, 2005) models also predict that older debris disks systems possess infrared bright rings of dust at larger radii than their younger counterparts. Since the dust grains in our sample probably have $a > 10$ μm, we plot the inferred blackbody dust distance, D, as a function of stellar age to test this hypothesis (see Fig. 6*b*). The blackbody distances, inferred from SED models, are consistent with the measured radii of HR 4796A, Fomalhaut, and Vega from maps of thermal emission from large particles at mid-infrared and submillimeter wavelengths to within a factor of 2 (Holland et al. 2003; Wilner et al. 2002; Jayawardhana et al. 1998). However, the blackbody distances are smaller than the measured radii of β Pic and AU Mic in scattered light (Krist et al. 2005; Heap et al. 2000) and smaller than the measured radius of Vega, inferred from maps of thermal emission of stochastically heated small grains (Su et al. 2005). We do not find a clear correlation between dust grain distance and the age of the central star, in agreement with submillimeter studies (Najita & Williams 2005). The addition of submillimeter data for η Crv and τ Cet does not appear to improve our fit of grain distance as a function of stellar age. In Figure 6*b*, we overplot grain distances for these objects inferred from submillimeter SED models.

7. CORRELATIONS BETWEEN STELLAR AND DUST PROPERTIES?

We searched for correlations between stellar and dust properties. We investigated whether the multiplicity, the rotational velocity, or the metallicity of the central star is correlated with either the observed fractional infrared luminosity or grain temperature.

In a binary system, the orbits of dust grains at distances approximately 1.6–2.6 times the binary separation are expected to be unstable (Artymowicz & Lubow 1994), leading to the formation of two populations of circumstellar dust grains. Disks around each component of the binary system are truncated at their outer radii, but cool dust may reside at much larger distances in circumbinary disks. We searched for a correlation between the single/binary nature of a stellar system and the inferred circumstellar dust properties (grain temperature and fractional infrared luminosity) to determine whether the gravitational effects of a secondary star affect disk properties.

Eleven stars in our sample are binary systems, five of which (45.5%) possess IRS excesses detected with good signal-to-noise ratios (SNRs). One of the binary systems with IRS excess does not possess spectral features and is better modeled using a single-temperature blackbody than a uniform disk whose surface density is given by Poynting-Robertson Drag (HR 1570). The grain temperature for this system is $T_{gr} = 90.6$ K and the fractional infrared luminosity for this system is 3.0×10^{-5}. For comparison, 49 stars in our sample are single systems, 29 of which (59.2%) possess IRS excesses detected with good SNRs. Fifteen of the single systems with IRS excesses do not possess spectral features and are better modeled using a single-temperature blackbody (HR 333, HR 506, γ Tri, HR 1082, HD 53143, HR 3314, HD 95086, HD 110058, λ Boo, HD 139664, HD 146897, HR 6297, HR 6486, HD 181327, and HD 191089). The mean grain temperature for these systems is $T_{gr} = 103$ K with a standard deviation of 19 K. The mean fractional infrared luminosity of these systems is 8.4×10^{-4} with a standard deviation of

TABLE 7

Binary Properties

Name	Primary and Secondary Spectral Types	Separation (arcsec)	Separation (AU)	Period (yr)	Notes	References
λ Cas	B7 V & B8 V	0.38	41	515	VB	2
HR 1570	A0 V & ?	40	1500			8
HR 1686	F6 V & ?	30	630			8
κ Lep	B7 V & B9 V	2.2	370			3, 6
32 Ori	B5 IV & B7 V	1.3	120	590	VB	1
HR 2124	A2 V & ?	0.1	5			5
ψ^5 Aur	G0 V & M0 V	31	520			8
G Cen	B3 Vn & ?	23	2800			8
HD 113766	F3/F5 V & ?	1.3	170			3
HR 6532	B9.5 V & <A9 V			0.019	SB	4
HR 7329	A0 Vn & M7/8 V	4	200	1700	CPM	7

Note.—(CPM) Common proper motion, (SB) spectroscopic binary, (VB) visual binary.

References.—(1) Abt & Cardona 1984; (2) Abt & Boonyarak 2004; (3) Fabricius & Makarov 2000; (4) Guthrie 1986; (5) Horch et al. 2002; (6) Lindroos 1985; (7) Lowrance et al 2000; (8) SIMBAD.

1.5×10^{-3}. The mean grain temperatures and fractional infrared luminosities for single and binary systems are consistent when the standard deviation of these quantities are taken into account.

One difference appears when the single and binary star populations are compared. The fraction of infrared excess binary systems that can be modeled by a single-temperature blackbody is significantly smaller than the number of infrared excess single-star systems. We list the angular and physical separation of all the binary systems in our sample in Table 7. One possibility for the poor single-temperature blackbody fits associated with binary systems is the presence of multiple populations of circumstellar dust grains (e.g., circumprimary, circumsecondary, and circumbinary disks). If the binary nature of these systems contributes to the complicated structure of the infrared excess, then objects that are not well modeled by a single-temperature blackbody should possess binary separations 1–100 AU. However, the separations of one of the two systems (λ Cas, HR 6532) that are not well modeled by a single-temperature blackbody is too small to truncate a circumstellar disk. HR 6532 is a spectroscopic binary with a period of 6.8 days. Larger statistics are needed to confirm whether the infrared spectra of binary systems are more complicated than a single-temperature blackbody.

We plot the fractional infrared luminosity and grain temperature as a function of binary separation (see Fig. 7) to examine

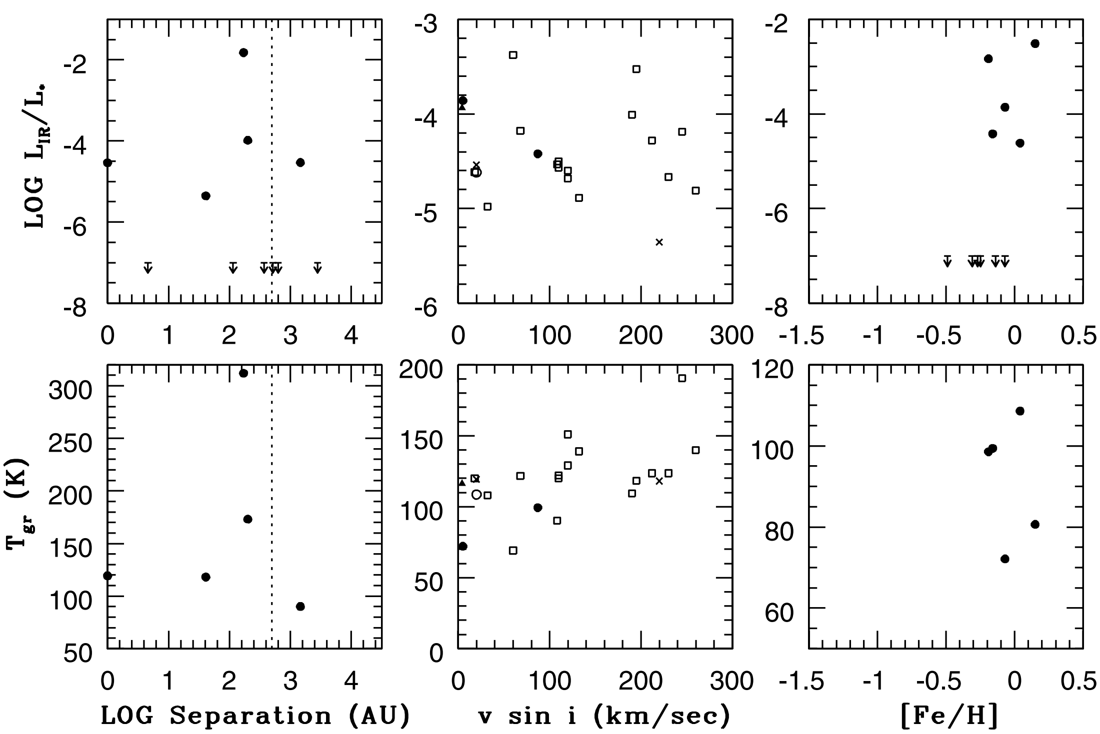

Fig. 7.—Inferred fractional luminosity, L_{IR}/L_*, and grain temperature, T_{gr}, plotted as a function of binary separation (for all binaries in our study), measured stellar rotational velocity, $v \sin i$, and stellar metallicity, [Fe/H]. For binary systems to the left of the dotted line, the LL (and sometimes the SL) slit contain both the primary and secondary; for objects to the right of the dotted vertical line, the SL and LL slits contain only the primary star. In plots of grain properties as a function of $v \sin i$ and [Fe/H], B-type stars are shown as crosses, A-type stars are shown as squares, F-type stars are shown as circles, and K-type stars are shown as triangles. Stars with spectral type earlier than F5 V are shown as open symbols in $v \sin i$ plots. Stars with spectral type earlier than F0 V are shown with open symbols in [Fe/H] plots.

further the effects of a secondary star. We assume very small separations for Algol eclipsing and spectroscopic binaries (<1 AU). Systems to the left of the dotted vertical line have separations $<10''$, small enough that both the primary and secondary fall into the LL (and sometimes the SL) slit. Systems to the right of the dotted vertical line are too widely separated for the secondary to contribute to either the SL or LL spectrum. The average fractional infrared luminosity for systems with separations of 10–100 AU, 1.6×10^{-5}, is smaller than that inferred for objects with separations of 100–500 AU, 7.6×10^{-4}; however, this comparison is highly biased by the very high fractional infrared luminosity associated with HD 113766, 1.5×10^{-2}, because our binary sample is so small. The average grain temperature for systems with separations of 10–100 AU, 120 K, is consistent with the peak in grain temperature distribution for the whole sample, but smaller than that inferred for systems with separations of 100–500 AU, 240 K. Debris disks with $T_{gr} \sim 250$ K are rare (Aumann & Probst 1991). The very high average T_{gr} estimated is based on a sample of two unusual objects (HD 113766 and η Tel). Detailed modeling of the 10 μm feature observed toward these objects suggests blackbody grains with $T_{gr} > 300$ K and amorphous olivine with $T_{gr} > 200$ K (see § 4; Schutz et al. 2005).

X-ray studies of solar-like stars suggest that magnetic breaking causes stars to rotate more slowly as they age, with a $v_{rot} \propto t^{-0.6\pm0.1}$ time dependence for stars with ages >0.3 Gyr (Ayres 1997). We searched for correlations between the inferred circumstellar dust properties and the measured projected stellar rotational velocity, $v \sin i$. Using $v \sin i$ as a proxy for stellar age, we expect that both the fractional infrared luminosity and the grain temperature will decrease with stellar age or increase with $v \sin i$. We plot the fractional infrared luminosity and grain temperature as a function of $v \sin i$ in Figure 7, using different symbols for B-, A-, F-, and K-type stars. For binary systems, we used the $v \sin i$ for the primary star. Stars with spectral type earlier than F5 Vare shown with open symbols, while stars with spectral type F5 Vand later are shown with solid symbols. Early-type stars are not expected to spin down as they age because they do not possess deep convective envelopes. When F5 V and later spectral-type stars in our sample are compared with one another, a possible decrease in fractional infrared luminosity as a function of $v \sin i$ and increase in grain temperature as a function of $v \sin i$ are seen. However, our sample is predominantly B- and A-type stars and only contains 3 mid-F and later type stars with measured dust grain properties and measured $v \sin i$; therefore, no strong conclusions about the dependence of dust grain properties on $v \sin i$ can be drawn in this study.

Radial velocity studies of main-sequence stars that possess giant planets find a correlation between the presence of an orbiting planet and the metallicity of the central star. Spectral synthesis modeling of high-resolution visual spectra, sensitive to stellar semiamplitudes >30 m s^{-1} and orbital periods shorter than 4 yr, find that fewer than 3% of stars with $-0.5 <$ [Fe/H] < 0.0 have Doppler-detected planets, while 25% of stars with [Fe/H] $> +0.3$ possess giant planets (Fischer & Valenti 2005). Recent *Spitzer* MIPS observations suggest that nearby planet-bearing, solar-like stars may be more likely to possess 70 μm excesses and larger average 70 μm excesses than stars without known planets (Beichman et al. 2005). These excesses are generated by cool dust ($T_{gr} < 100$ K) located beyond 10 AU, well outside the orbits of the discovered planets. If correlations exist between metallicity and the presence of a planet and between the presence of a planet and a 70 μm excess, there might also be a correlation between the presence of IRS excess and stellar metallicity, although no correlations between the presence of 70 μm excess and stellar metallicity have been found thus far (Bryden et al. 2006; Beichman et al. 2005).

We plot fractional infrared luminosity and grain temperature versus [Fe/H] for the 11 F-type stars in our sample that possess [Fe/H] measurements determined from the Strömgren photometry survey of Nordstrom et al. (2004; see Fig. 7). For the six objects that do not possess IRS excess, we indicate their position along [Fe/H] axis with an upper limit symbol. The stars with and without detected IRS excess have similar metallicities, consistent with a stochastic origin for the small infrared emitting grains in debris disks. We do not include B- and A-type stars in this plot because they possess shallow surface convective zones. The observed metallicity of these objects may be more easily distorted by pollution than their F-type counterparts. We observe a large dispersion in both the fractional infrared luminosity and grain temperature even though our sample only contains 5 F-type stars with measured grain properties and measured [Fe/H]. More objects from our sample may be folded in when grain properties inferred from longer wavelength observations are included; for example, τ Cet, with [Fe/H] $= -0.47$, $\log (L_{IR}/L_*) = -4.6$ (Decin et al. 2003), and $T_{gr} = 60$ K (Greaves et al. 2004) inferred from far-infrared and submillimeter photometry.

8. GAS MASS UPPER LIMITS

Atomic and molecular gases may affect the dynamics of circumstellar dust grains. Numerical models of disks with gas-to-dust ratios of 0.1–10 suggest that gas-grain interactions may generate the observed infrared bright rings by concentrating small grains, with radii just above the blowout radius, at the outer edge of the gas disk (Takeuchi & Artymowicz 2001). In addition, measurement of gas masses in a large sample of disks may help determine the gas dissipation timescale and help constrain models for giant planet formation (Hollenbach et al. 2005). We searched for H_2 $S(0)$, $S(1)$ and S I emission at 28.2, 17.0, and 25.2 μm, respectively, to constrain the bulk gas mass in debris disks. We do not detect any of these emission lines in any of our SH and LH module data. We estimate 3 σ upper limits to the H_2 $S(0)$, $S(1)$ and S I line fluxes from our nod difference spectra (see Table 8). Since the amplitude of each difference spectrum varied from pixel to pixel near each line, we averaged each difference spectrum in a region ±0.5 μm around each line to determine the uncertainty in the line flux. We estimate H_2 mass upper limits from the $S(0)$ line flux upper limits, assuming that the source is unresolved and that the gas has a temperature $T_{ex} = 50$ and 100 K, expected from bulk gas that is cospatial with the infrared-emitting dust. Since the most constraining gas mass upper limits are typically <100 $M_\oplus$ and the measured submillimeter dust masses are typically <1 $M_\oplus$, we cannot constrain the gas-to-dust ratio in debris disks well.

Molecular gas has been detected toward the nearby (70 pc away from the Sun) $\sim$20 Myr old star 49 Cet. Submillimeter observations find CO $J = 3 \rightarrow 2$ and $J = 2 \rightarrow 1$ emission at the radial velocity of the star (Dent et al. 2005; Zuckerman et al. 1995). Models of the 49 Cet doubly peaked CO $J = 3 \rightarrow 2$ profile are consistent with a compact disk with an outer radius, $D_{out} = 17$ AU, and a disk inclination, $i = 16°$; the high-velocity wings of the profile ($\sim$4 km s^{-1} relative to the star) suggest that gas is present at $\leq$5 AU from the central star (Dent et al. 2005). *ISO* observations detect H_2 $S(0)$ and $S(1)$ emission with a line flux $(6.6 \pm 2.0) \times 10^{-14}$ ergs s^{-1} cm^{-2} and place 3 σ upper limits on the $S(1)$ line flux, $<0.8 \times 10^{-14}$ ergs s^{-1} cm^{-2}, corresponding to a gas-to-dust ratio >100 (Thi et al. 2001). Our 49 Cet 3 σ

TABLE 8
Emission Line and Gas Mass 3 σ Upper Limits

Name	H_2 $S(1)$ (erg s^{-1} cm^{-2})	S i (erg s^{-1} cm^{-2})	H_2 $S(0)$ (erg s^{-1} cm^{-2})	50 K M_{H_2} ($M_\oplus$)	100 K M_{H_2} ($M_\oplus$)
49 Cet	$<8.6 \times 10^{-15}$	$<1.0 \times 10^{-14}$	$<7.4 \times 10^{-15}$	<6000	<80
τ Cet	$<2.7 \times 10^{-13}$	$<3.2 \times 10^{-14}$	$<1.9 \times 10^{-14}$	<70	<1
τ^3 Eri	$<5.0 \times 10^{-15}$	$<1.5 \times 10^{-14}$	$<5.8 \times 10^{-15}$	<900	<10
α For	$<4.3 \times 10^{-14}$	$<1.4 \times 10^{-14}$	$<1.3 \times 10^{-14}$	<600	<7
ζ Lep	$<2.1 \times 10^{-14}$	$<1.8 \times 10^{-14}$	$<1.0 \times 10^{-14}$	<1000	<10
HR 2124	$<2.3 \times 10^{-14}$	$<7.7 \times 10^{-15}$	$<1.1 \times 10^{-14}$	<5000	<70
δ Vel	$<5.0 \times 10^{-14}$	$<1.2 \times 10^{-14}$	$<4.2 \times 10^{-15}$	<500	<7
β UMa	$<1.9 \times 10^{-14}$	$<7.3 \times 10^{-15}$	$<3.8 \times 10^{-15}$	<500	<6
β Leo	$<2.5 \times 10^{-14}$	$<6.1 \times 10^{-14}$	$<4.4 \times 10^{-14}$	<1000	<10
η Crv	$<2.3 \times 10^{-14}$	$<1.2 \times 10^{-14}$	$<8.9 \times 10^{-15}$	<600	<8
HD 113766	$<1.1 \times 10^{-13}$	$<2.1 \times 10^{-14}$	$<1.0 \times 10^{-14}$	<40000	<500
γ Tra	$<2.7 \times 10^{-14}$	$<1.4 \times 10^{-14}$	$<9.3 \times 10^{-15}$	<7000	<80
α CrB	$<3.0 \times 10^{-14}$	$<1.3 \times 10^{-14}$	$<6.5 \times 10^{-15}$	<800	<10
41 Ser	$<3.7 \times 10^{-14}$	$<1.3 \times 10^{-14}$	$<8.0 \times 10^{-15}$	<200	<3
HR 6486	$<2.6 \times 10^{-14}$	$<1.0 \times 10^{-14}$	$<9.0 \times 10^{-15}$	<1000	<20
γ Oph	$<1.3 \times 10^{-14}$	$<1.9 \times 10^{-14}$	$<6.4 \times 10^{-15}$	<1000	<20
HR 7012	$<2.4 \times 10^{-14}$	$<1.1 \times 10^{-14}$	$<1.3 \times 10^{-14}$	<2400	<30

H_2 $S(0)$ line flux upper limit apparently conflicts with the Thi et al. (2001) results because our $S(0)$ upper limit is a factor $\sim$9 lower than the reported detection. Our upper limit is consistent with the mass expected in H_2 inferred from 800–1100 μm continuum measurements of the dust mass, $M_{\rm submm} = 0.02{-}1\ M_\oplus$, if the disk has an interstellar gas-to-dust ratio (Zuckerman et al. 1995) and is also consistent with the inferred CO masses from submillimeter measurements. Zuckerman et al. (1995) and Dent et al. (2005) estimate that between 2 and 30 $M_\oplus$ H_2 exists in the disk, assuming a gas excitation temperature $T_{\rm ex} = 50{-}60$ K and an interstellar H_2:CO number ratio between 1×10^4 and 2×10^4, significantly smaller than the <6000 and <80 $M_\oplus$ that we infer assuming $T_{\rm ex} = 50$ and 100 K, respectively.

The nondetection of H_2 emission at mid-infrared wavelengths using *Spitzer* IRS may be somewhat constraining for at least one object in our sample. The expected H_2 emission line luminosity may be estimated from our inferred parent body masses (using the estimates in Table 5) assuming an interstellar gas-to-dust ratio and a gas excitation temperature $T_{\rm ex} = T_{\rm gr}$. If the system is a point source, then the total luminosity produced by $N(H_2)$ H_2 molecules is

$$F = \frac{h\nu N(H_2)\chi_u A_{ul}}{4\pi d^2}, \tag{14}$$

where $E = h\nu$ is the energy of the radiated photons, χ_u is the fraction of H_2 in level u, and A_{ul} is the transition probability. HD 113766 is a F3/F5 V member of Lower Centaurus Crux in Scorpius-Centaurus, with an estimated age of 16 Myr and a notably large $L_{\rm IR}/L_* = 0.015$ (Chen et al. 2005). In our high-resolution mode sample, HD 113766 possesses the largest parent body mass (0.1 $M_\oplus$ or 260 times that mass in the main asteroid belt) and the hottest single blackbody grain temperature, $T_{\rm gr} = 330$ K, making it the most likely object to possess H_2 $S(0)$ and $S(1)$ emission. The approximation $T_{\rm ex} = T_{\rm gr}$ is valid for optically thick, flared disks for $A_V > 0.1$ (Kamp & Dullemond 2004) but invalid for debris disks around A-type stars where the disk gas and dust are too tenuous to heat the gas via gas-grain collisions (Kamp & van Zadelhoff 2001). For example, modeling of the gas around HR 4796A, an 8 Myr old A-type member of the TW Hydrae Association, located 67 pc away from the Sun, suggests that the gas, $T_{\rm ex} = 65$ K, is substantially cooler than the dust, $T_{\rm gr} = 110$ K (Chen & Kamp 2004). With these caveats, we estimate that the HD 113766 disk should possess H_2 $S(0)$ and $S(1)$ line fluxes of 2.8×10^{-15} ergs s^{-1} cm^{-2} and 2.8×10^{-13} ergs s^{-1} cm^{-2}, respectively, corresponding to an $S(1)$ emission line flux $\sim$3 times higher than our observed 3 σ upper limit.

Gorti & Hollenbach (2004) have argued that [S i] emission at 25.2 μm may be an excellent tracer for bulk gas in protoplanetary disks. Their model spectra of disks around intermediate-aged ($\sim 10^7$ years) stars predicts strong [S i] emission, with line-to-continuum ratios >5% in *Spitzer* IRS high-resolution mode ($R \sim 600$), assuming that the disk sulfur abundance is similar to that observed in the diffuse interstellar medium (2.8×10^{-5}) because cospatial dust grains are too warm for volatiles to condense on them. However, the gas-phase sulfur abundance in intermediate-aged disks may be depleted relative to the diffuse interstellar medium. The previously identified 23.5 μm wüstite (FeO) emission feature detected in *ISO* spectra of Herbig Ae stars may not be wüstite but pyrrhotite ($[{\rm Fe, Ni}]_{1-x}$S). Keller et al. (2002) compare the intrinsic strength of the 18 μm silicate feature to that of the 23.5 μm pyrrhotite feature in the *ISO* spectrum of HD 163496 and measure a silicon-to-sulfur ratio of 0.63, consistent with a solar abundance (0.52). They conclude that most if not all of the sulfur around HD 163296 resides in solid FeS grains. If the bulk of the circumstellar sulfur is located in grains, then [S i] emission at 25.2 μm (or lack thereof) may not be a good bulk gas tracer.

9. CONCLUSIONS

We have obtained *Spitzer Space Telescope* IRS spectra of 59 main-sequence stars with spectral types B through M and ages between 1 Myr and a few Gyr that possess *IRAS* 60 μm excess. We find the following:

1. The majority of observed debris disks do not possess spectral features, suggesting that the grains are too cold and/or too large ($a \geq 10$ μm) to produce spectral features. Detailed modeling of objects with spectral features requires the presence of large,

warm amorphous silicates with $T_{gr} = 290-600$ K, in addition to cool blackbody grains with $T_{gr} = 80-200$ K, and the presence of crystalline silicate mass ratios 0%–76%.

2. The IRS spectra of debris disks (without spectral features) are generally better fitted using a single-temperature blackbody than with a uniform disk. Stellar radiation pressure (in collisionally dominated systems), sublimation if the grains are icy, gas drag, and/or the presence of a perturbing body may contribute to the presence of inner holes in these disks.

3. The peak in the distribution of estimated blackbody grain temperatures, $T_{gr} = 110-120$ K, suggesting that sublimation of icy grains may produce the central clearings observed.

4. Since the parent body masses typically are less than the mass of the Earth, it appears that planet formation efficiently consumes most of the mass of the primordial disk.

We would like to thank K. Uchida for his assistance with data reduction and our anonymous referee, S. Kenyon, E. Mamajek, J. Mould, I. Song, A. Speck, K. Stapelfeldt, and S. Strom for their helpful comments and suggestions. This material is based on work supported by the National Aeronautics and Space Administration under Award NAS7-1407 and the California Institute of Technology.

APPENDIX

SELECTED SOURCE NOTES

HR 506 may possess a planet with a period of 1040 days, a minimum ($M \sin i$) mass of 0.91 $M_{\rm Jup}$, and a Doppler velocity semiamplitude of 18 m s^{-1}; the inferred eccentricity and semimajor axis for the planetary orbit are $e = 0.18$ and $a = 2.1$ AU (Butler et al. 2006). If HR 506 possesses blackbody grains at a distance $D = 2.1$ AU from the star, then they are expected to have a grain temperature of $T_{gr} = 220$ K, assuming a stellar radius $R_* = 1.2\ R_\odot$ and an effective temperature $T_{\rm eff} = 6140$ K, consistent with a stellar spectral type of F8 V. However, the IRS excess continuum emission observed toward this star is better fitted by a blackbody with a cooler grain temperature $T_{gr} = 70$ K, suggesting that planetesimals at similar distances have already been removed. The blackbody distance for $T_{gr} = 70$ K grains is $D = 21$ AU. Therefore, the observed infrared emitting dust and parent body population are located at significantly larger distances than the radial velocity planet. A second planet in this system is probably needed to dynamically stir the parent bodies because the observed radial velocity planet is located too far away to generate strong orbital resonances (Bryden et al. 2000; Beichman et al. 2006).

τ Cet is a 7.2 Gyr old G8 V star (Lachaume et al. 1999) that possesses *IRAS* and JCMT SCUBA excesses that are well fitted by a $T_{gr} = 60$ K modified blackbody (Greaves et al. 2004). However, the thermal emission from this cold dust population is not well detected at IRS wavelengths ($\lambda < 35\ \mu$m). The slope of the 20–35 μm IRS spectrum is expected to be ~4% higher assuming the Greaves et al. (2004) model. The difficulty in detecting thermal emission from this population of circumstellar grains suggests that the IRS is sensitive to grains with dust temperature $T_{gr} > 60$ K.

HR 3927 is a A0 V star with an estimated age of 50 Myr. Its *Spitzer* IRS spectrum possesses a 10 μm feature that may be modeled using solid amorphous olivine and crystalline forsterite grains with $a = 3.1$ and 8 μm, respectively, larger than the blowout size for both species, $T_{gr} = 290$ K, and a crystalline silicate fraction of 38%. The residual continuum emission may be modeled using blackbody grains with a lower grain temperature $T_{gr} = 80$ K. The presence of a cooler blackbody continuum in addition to the hot silicate grains suggests that this system possesses two planetesimal belts analogous to the asteroid and Kuiper belts in our solar system. The *IRAS* (not color-corrected) 60 μm flux of 0.69 Jy is somewhat higher than the 0.34 Jy inferred from our model; however, the presence of a second source in the beam cannot be ruled out without *Spitzer* MIPS images. If HR 3927 does possess a larger 60 μm excess than predicted by our model, then it may also possess an additional (or third) population of cold dust with $T_{gr} < 60$ K.

η Crv is a F2 V star with an estimate age of 1 Gyr based on its X-ray activity. This system may possess three populations of dusty debris. The coldest population with $T_{gr} = 40 \pm 5$ K has been detected at submillimeter wavelengths where the system is resolved at all position angles at 450 μm with an elongation at a position angle of $130° \pm 10°$ and at 850 μm with a radius of 100 AU (Wyatt et al. 2005). A second component is detected in *IRAS* photometry; self-consistent modeling of the *IRAS* and submillimeter photometry suggest that this population possesses a grain temperature $T_{gr} = 370 \pm 60$ K (Wyatt et al. 2005). Detailed fits to the *Spitzer* IRS 5.5–35 μm spectra suggest that this emission is produced by amorphous olivine, and crystalline forsterite and enstatite features with $T_{gr} = 360$ K and a crystalline silicate fraction of 31%, and blackbody grains with a temperature $T_{gr} = 120$ K. The detection of three planetesimal belts may require the presence of at least two perturbing planets because three belts are unlikely to be located at the resonances of a single planet. Detailed dynamical models of this system are required to determine whether η Crv possesses multiple planets.

HD 113766 is a binary member of Lower Centaurus Crux in the Sco-Cen OB Association with an estimated age of ~16 Myr (Mamajek et al. 2002). The secondary lies 1.″3 (or 170 AU) away from the F3/F5 primary. HD 113766 possesses an extremely high fractional infrared luminosity $L_{\rm IR}/L_* = 1.5 \times 10^{-2}$ and MIPS 24 and 70 μm fluxes that are well fitted with a $T_{gr} = 330$ K blackbody, suggestive of debris at terrestrial planet temperatures (Chen et al. 2005). Published ground-based ESO TIMMI2 spectra suggest that the 10 μm feature is dominated by crystalline silicate (forsterite) and large, amorphous silicates; SiO_2, which is correlated with the presence of forsterite in Herbig AeBe *ISO* spectra, is not detected (Schütz et al. 2005). We use crystalline forsterite in addition to amorphous carbon, olivine, and pyroxene, and a single-temperature blackbody to fit not just the 10 μm feature but also the 5.5–35 μm IRS spectrum and infer a crystalline silicate fraction of 4.1%. The presence of a cooler blackbody continuum ($T_{gr} = 200$ K) in addition to the hot silicate and carbon grains ($T_{gr} = 600$ K) suggests that this system possesses two planetesimal belts analogous to the asteroid and Kuiper belts in our solar system. The lack of spectral features due to sub-micron–sized grains can be explained if small particles are radiatively driven from the system by radiation pressure.

μ Ara possesses a planet with a period of 743 days, a minimum ($M \sin i$) mass of 1.97 $M_{\rm Jup}$, and a Doppler velocity semiamplitude of 54 m s^{-1}; the inferred eccentricity and semimajor axis for the planetary orbit are $e = 0.62$ and $a = 1.65$ AU (Butler et al. 2006). If the system possessed blackbody grains at a distance $D = 1.65$ AU from the star, then they would have a grain temperature of

$T_{gr} = 220$ K, assuming a stellar radius $R_* = 0.99\,R_\odot$ and an effective temperature $T_{eff} = 5830$ K, consistent with a stellar spectral type of G3 V. Grains with such high temperatures are expected to produce a blackbody continuum that peaks near 25 μm in the center of the IRS bandpass, similar to that observed toward ζ Lep. However, no excess emission has been detected toward μ Ara at IRS wavelengths. One possible explanation for the lack of infrared excess is that this system has already destroyed any planetesimal belt it may have possessed by its estimated age of 6.2 Gyr (Lachaume et al. 1999).

HR 7012 is a A5 IV–V member of the β Pic moving group with an estimated age of 12 Myr (Zuckerman et al. 2001). Its *Spitzer* IRS spectrum possesses a strong 10 μm silicate feature that may be modeled using large amorphous olivine and pyroxene grains with $a = 5.0$ and 1.1 μm, respectively, and $T_{gr} = 520$ K and sub-micron–sized crystalline enstatite and cristobalite. Cristobalite is used to fit emission in the shoulder of the silicate feature at $\lambda < 8.7$ μm; however, other materials such as opal (hydrated silica) may also provide acceptable fits. We estimate that this system possesses a crystalline silicate fraction of 76%; however, our model produces extra emission at 10.5 and 19.5 μm that may indicate that the fraction of crystalline pyroxene used is too high. The presence of small sub-micron–sized grains inferred from our fit to the HR 7012 spectrum suggest that this system may have experienced a recent collision.

η Tel is a binary member of the β Pic moving group with an estimated age of 12 Myr (Zuckerman et al. 2001). The M7/8 V secondary located at a distance of 4″ (or 200 AU) away from the A0 V primary was detected via common proper motion studies (Lowrance et al. 2000). The η Tel *Spitzer* IRS spectrum possesses a 10 μm feature that may be modeled using solid amorphous olivine grains with $a = 3.0$ μm, larger than the blowout size, and $T_{gr} = 370$ K. The residual continuum emission may be modeled using blackbody grains with a lower temperature $T_{gr} = 115$ K. The presence of a cooler blackbody continuum in addition to the hot silicate grains suggests that this system possesses two planetesimal belts analogous to the asteroid and Kuiper belts in our solar system. This spectrum does not appear to possess crystalline forsterite or enstatite features despite the young age of the system. For comparison, HR 7012 (another A-type member of the β Pic moving group) has a crystalline silicate fraction of 76%.

REFERENCES

Abt, H. A., & Boonyarak, C. 2004, ApJ, 616, 562
Abt, H. A., & Cardona, O. 1984, ApJ, 285, 190
Aumann, H. H., & Probst, R. G. 1991, ApJ, 368, 264
Artymowicz, P. 1988, ApJ, 335, L79
Artymowicz, P., & Lubow, S. H. 1994, ApJ, 421, 651
Ayres, T. R. 1997, J. Geophys. Res., 102, 1641
Backman, D. E., & Paresce, F. 1993, in Protostars and Planets III, ed. E. Levy & J. I. Lunine (Tuscon: Univ. Arizona Press), 1253
Beichman, C. A., et al. 2005, ApJ, 622, 1160
———. 2006, ApJ, 639, 1166
Bhatt, H. C. 2000, A&A, 362, 715
Bohren, C. F., & Huffman, D. R. 1983, Absorption and Scattering of Light by Small Particles (New York: Wily)
Bouwman, J., Meeus, G., de Koter, A., Hony, S., Dominik, C., & Waters, L. B. F. M. 2001, A&A, 375, 950
Bryden, G., Lin, D. N. C., & Ida, S. 2000, ApJ, 544, 481
Bryden, G., et al. 2006, ApJ, 636, 1098
Burns, J. A., Lamy, P. L., & Soter, S. 1979, Icarus, 40, 1
Butler, R. P., et al. 2006, ApJ, 646, 505
Cardelli, J. A., Clayton, G. C., & Mathis, J. S. 1989, ApJ, 345, 245
Chen, C. H., & Jura, M. 2001, ApJ, 560, L171
Chen, C. H., Jura, M., Gordon, K. D., & Blaylock, M. 2005, ApJ, 623, 493
Chen, C. H., & Kamp, I. 2004, ApJ, 602, 985
Chihara, H., Koike, C., Tsuchiyama, A., Tachibana, S., & Sakamoto, D. 2002, A&A, 391, 267
Coté, J. 1987, A&A, 181, 77
Cutri, R. M., et al. 2003, 2MASS All-Sky Catalog of Point Sources (Pasadena: IPAC/Caltech)
de Zeeuw, P. T., Hoogerwerf, R., de Bruijne, J. H. J., Brown, A. G. A., & Blaauw, A. 1999, AJ, 117, 354
Decin, G., Dominik, C., Waters, L. B. F. M., & Waelkens, C. 2003, ApJ, 598, 636
Dent, W. R. F., Greaves, J. S., & Coulson, I. M. 2005, MNRAS, 359, 663
Dominik, C., & Decin, G. 2003, ApJ, 598, 626
Dorschner, J., Begemann, B., Henning, T., Jaeger, C., & Mutschke, H. 1995, A&A, 300, 503
Fabian, D., Henning, T., Jager, C., Mutschke, H., Dorschner, J., & Wehrhan, O. 2001, A&A, 378, 228
Fabricius, C., & Makarov, V. V. 2000, A&A, 356, 141
Figueras, F., & Blasi, F. 1998, A&A, 329, 957
Fischer, D. A., & Valenti, J. 2005, ApJ, 622, 1102
Fleming, T. A., Schmitt, J. H. M. M., & Giampapa, M. S. 1995, ApJ, 450, 401
Flower, P. J. 1996, ApJ, 469, 355
Ford, K. E., & Neufeld, D. A. 2001, ApJ, 557, L113
Forrest, W. J., et al. 2004, ApJS, 154, 443
Fraser, H. J., Collings, M. P., McCoustra, M. R. S., & Williams, D. A. 2001, MNRAS, 327, 1165
Gorti, U., & Hollenbach, D. 2004, ApJ, 613, 424
Greaves, J. S., Wyatt, M. C., Holland, W. S., & Dent, W. R. F. 2004, MNRAS, 351, L54
Greenberg, R., & Nolan, M. C. 1989, in Asteroids II, ed. R. P. Binzel, T. Gehrels & M. S. Matthews (Tuscon: Univ. Arizona Press), 778
Grosbol, P. J. 1978, A&AS, 32, 408
Guthrie, B. N. G. 1986, MNRAS, 220, 559
Heap, S. R., Lindler, D. J., Lanz, T. M., Cornett, R. H., Hubeny, I., Maran, S. P., & Woodgate, B. 2000, ApJ, 539, 435
Higdon, S. J. U., et al. 2004, PASP, 116, 975
Holland, W. S., et al. 2003, ApJ, 582, 1141
Hollenbach, D., et al. 2005, ApJ, 631, 1180
Holmes, E. K., Butner, H. M., Fajardo-Acosta, S. B., & Rebull, L. M. 2003, AJ, 125, 3334
Honda, M., Kataza, H., Okamoto, Y. K., Miyata, T., Yamashita, T., Sako, S., Takubo, S., & Onaka, T. 2003, ApJ, 585, L59
Horch, E. P., Robinson, S. E., Meyer, R. D., van Altena, W. F., Ninkov, Z., & Piterman, A. 2002, AJ, 123, 3442
Houck, J. R., Roellig, T. L., van Cleve, J., Forrest, W. J., Herter, T., Lawrence, C. R., Matthews, K., & Reitsema, H. J. 2004, ApJS, 154, 18
Jaeger, C., Molster, F. J., Dorschner, J., Henning, T., Mutschke, H., & Waters, L. B. F. M. 1998, A&A, 339, 904
Jayawardhana, R., Fisher, R. S., Hartmann, L., Telesco, C., Pina, R., & Fazio, G. 1998, ApJ, 503, L79
Johnson, H. L., Mitchell, R. I., Iriarte, B., & Wisniewski, W. Z. 1966, Commun. Lunar Planet. Lab. 4, 99
Jura, M. 2004, ApJ, 603, 729
Jura, M., Ghez, A. M., White, R. J., McCarthy, D. W., Smith, R. C., & Martin, P. G. 1995, ApJ, 445, 451
Jura, M., Malkan, M., White, R., Telesco, C., Pina, R., & Fisher, R. S. 1998, ApJ, 505, 897
Jura, M., et al. 2004, ApJS, 154, 453
Kalas, P., & Graham, J. R. 2002, ApJ, 567, 999
Kessler-Silacci, J., et al. 2006, ApJ, 639, 275
Krivov, A. V., Mann, I., & Krivova, N. A. 2000, A&A, 362, 1127
Kamp, I., & Dullemond, K. 2004, ApJ, 615, 991
Kamp, I., & van Zadelhoff, G. J. 2001, A&A, 373, 641
Keller, L. P., et al. 2002, Nature, 417, 148
Kenyon, S. J., & Bromley, B. C. 2004, AJ, 127, 513
———. 2005, AJ, 130, 269
Koike, C., Chihara, H., Tsuchiyama, A., Suto, H., Sogawa, H., & Okuda, H. 2003, A&A, 399, 1101
Krist, J. E., et al. 2005, ApJ, 129, 1008
Lachaume, R., Dominik, C., Lanz, T., & Habing, H. J. 1999, A&A, 348, 897
Lagrange, A.-M., Backman, D. E., & Artymowicz, P. 2000, in Protostars and Planets IV, ed. V. Mannings, A. P. Boss, & S. S. Russell (Tuscon: Univ. Arizona Press), 639
Lindroos, K. P. 1985, A&AS, 60, 183
Liou, J., & Zook, H. A. 1999, AJ, 118, 580
Lowrance, P. J., et al. 2000, ApJ, 541, 390
Mamajek, E. E., Meyer, M. R., & Liebert, J. 2002, AJ, 124, 1670
Mannings, V., & Barlow, M. J. 1998, ApJ, 497, 330

Mermilliod, J.-C., Mermilliod, M., & Hauck, 1997, A&AS, 124, 349
Najita, J., & Williams, J. P. 2005, ApJ, 635, 625
Napiwotzki, R., Schonberber, D., & Wenske, V. 1993, A&A, 268, 653
Nordstrom, B., et al. 2004, A&A, 418, 989
Paunzen, E. 1997, A&A, 326, L29
Plavchan, P., Jura, M., & Lipscy, S. J. 2005, ApJ, 631, 1161
Pollack, J. B., Hubickyj, O., Bodenheimer, P., Lissauer, J. J., Podolak, M., & Greenzweig, Y. 1996, Icarus, 124, 62
Quillen, A. C., & Thorndike, S. 2002, ApJ, 578, L149
Reach, W. T., Morris, P., Boulanger, F., & Okumura, K. 2003, Icarus, 164, 384
Rieke, G. H., et al. 2005, ApJ, 620, 1010
Sadakane, K., & Nishida, M. 1986, PASP, 98, 685
Sargent, B., et al. 2006, ApJ, submitted
Schaller, G., Schaerer, D., Meynet, G., & Maeder, A. 1992, A&AS, 96, 269
Schütz, O., Meeus, G., & Sterzik, M. F. 2005, A&A, 431, 175
Sheret, I., Ramsay Howat, S. K., & Dent, W. R. F. 2003, MNRAS, 343, L65
Siess, L., Dufour, E., & Forestini, M. 2000, A&A, 358, 593
Simon, I., & McMahon, H. O. 1953, J. Chem. Phys., 21, 23
Sloan, G. C., et al. 2004, ApJ, 614, L77
Song, I., Caillault, J.-P., Barrado y Navascués, D., & Stauffer, J. 2001, ApJ, 546, 352
Song, I., Caillault, J.-P., Barrado y Navascués, D., Stauffer, J., & Randich, S. 2000, ApJ, 533, L41
Strom, R. G., Malhotra, R., Ito, T., Yoshida, F., & Kring, D. A. 2005, Science, 309, 1847
Strubbe, L. E., & Chiang, E. I. 2006, ApJ, submitted (astro-ph/0510527)
Su, K. Y. L., et al. 2005, ApJ, 628, 487
Sylvester, R. J., Skinner, C. J., Barlow, M. J., & Mannings, V. 1996, MNRAS, 279, 915
Takeuchi, T., & Artymowicz, P. 2001, ApJ, 557, 990
Thi, W. F., et al. 2001, ApJ, 561, 1074
Thompson, G. I., Nandy, K., Jamar, C., Monfils, A., Houziaux, L., Carnochan, D. J., & Wilson, R. 1978, Catalog of Stellar Ultraviolet Fluxes (ESA SR-28; Noordwijk: ESA)
Uchida, K. I., et al. 2004, ApJS, 154, 439
Vink, J. S., de Koter, A., & Lamers, H. J. G. M. 2000, A&A, 362, 295
Walker, H., & Wolstencroft, R. D. 1988, PASP, 100, 1509
Watson, D. W., et al. 2004, ApJS, 154, 391
Werner, M. W., et al. 2004, ApJS, 154, 1
Wilner, D. J., Holman, M. J., Kuchner, M. J., & Ho, P. T. P. 2002, ApJ, 569, L115
Wood, B. E., Muller, H.-R., Zank, G. P., & Linsky, J. L. 2002, ApJ, 574, 412
Wood, B. E., Muller, H.-R., Zank, G. P., Linsky, J. L., & Refield, S. 2005, ApJ, 623, L143
Wyatt, M. C. 2005, A&A, 433, 1007
Wyatt, M. C., Greaves, J. S., Dent, W. R. F., & Coulson, I. M. 2005, ApJ, 620, L492
Zubko, V. G., Mennella, V., Colangeli, L., & Bussoletti, E. 1996, MNRAS, 282, 1321
Zuckerman, B. 2001, ARA&A, 39, 549
Zuckerman, B., Forveille, T., & Kastner, J. 1995, Nature, 373, 494
Zuckerman, B., & Song, I. 2004, ApJ, 603, 738
Zuckerman, B., Song, I., Bessell, M. S., & Webb, R. A. 2001, ApJ, 562, L87